Universidade do Minho
Escola de Engenharia

Tiago Joaquim Ferreira da Costa

Development and validation of a bioradar for automotive mobility systems

March 2022

Development and validation of a bioradar for automotive mobility systems

Tiago Joaquim Costa

UMinho | 2022

Universidade do Minho
Escola de Engenharia

Tiago Joaquim Ferreira da Costa

Development and validation of a bioradar for automotive mobility systems

Master Thesis

Biomedical Engineering

Medical Electronics

Work developed under the supervision of:

Paulo Francisco da Silva Cardoso

Adriano Dídimo Machado de Carvalho

March 2022

Acknowledgments

I would like to thank my girlfriend Rita, my family, especially my mother, and my friends for all the support they gave me not only in the last year and a half, but throughout the entirety of my time studying in the University of Minho.

I would also like to thank my advisor Professor Paulo Cardoso, my co-advisor Adriano Carvalho, Professor Paulo Carvalhal and all others who were involved in this project for their help in making it come to fruition.

This work is supported by: European Structural and Investment Funds in the FEDER component, through the Operational Competitiveness and Internationalization Programme (COMPETE 2020) [Project nº 039334; Funding Reference: POCI-01-0247-FEDER-039334].

STATEMENT OF INTEGRITY

I hereby declare having conducted this academic work with integrity. I confirm that I have not used plagiarism or any form of undue use of information or falsification of results along the process leading to its elaboration.

I further declare that I have fully acknowledged the Code of Ethical Conduct of the University of Minho.

Resumo

Desenvolvimento e validação de um bioradar para sistemas de mobilidade automóvel

Neste estudo, múltiplos bioradares são estudados e testados num ambiente automóvel, com o objetivo de criar um sistema de deteção de sinais vitais que seja capaz de monitorizar o Ritmo Respiratório e Ritmo Cardíaco de passageiros em sistemas de mobilidade, tal como Veículos Autónomos Partilhados.

A pesquisa anterior neste tópico foca-se principalmente no seu uso em ambientes controlados, com apenas alguns estudos em ambientes automóveis, e apenas em monitorização do condutor. Monitorização de passageiros num ambiente automóvel é mais desafiante do que noutros ambientes devido a haver mais fontes de interferência, tais como o espaço fechado e movimento do veículo, e também é mais desafiante que monitorização do condutor, pois nesse caso o bioradar pode ser posto no volante ou abaixo dele, reduzindo a distância ao sujeito e restringindo o espaço detetado para incluir apenas o condutor.

Três bioradares foram testados, o primeiro sendo um bioradar pré-feito com capacidade de medir ritmo respiratório e cardíaco, e os dois últimos sendo baseados em módulos de radar disponíveis comercialmente, um radar de *Impulse-Response Ultra-Wide Band* e o outro um radar de *Frequency Modulated Continuous Wave*, para os quais múltiplas variações de *software* de deteção de sinais vitais foram desenvolvidas. Testes foram feitos numa carrinha, onde o primeiro bioradar foi usado para gravar medições de sinais vitais e os dois últimos foram usados para gravar dados brutos, enquanto um dispositivo foi usado para gravar os sinais vitais verdadeiros. Depois, o *software* desenvolvido foi usado para medir sinais vitais baseado nos dados brutos gravados pelos dois últimos radars, e a performance de cada bioradar e variação do *software* foi avaliada através de comparação com os sinais vitais verdadeiros.

Quando o veículo está parado, o radar de *Impulse-Response Ultra-Wide Band*, usando o método de *loopback filter*, teve a melhor performance de medição de ritmo respiratório (6.28 % de média do Erro Médio Relativo), e o radar de *Frequency Modulated Continuous Wave*, com definições para aumentar o *framerate*, e usando dados diferenciais e correção de fase, teve a melhor performance de medição de ritmo cardíaco (3.19 % de média de Erro Médio Relativo). Quando o veículo está em movimento, os resultados são mais inconsistentes e difíceis de avaliar. No geral, os resultados sugerem que monitorização de sinais vitais em ambiente automóvel usando bioradares é possível, mas necessita de mais pesquisa.

Palavras-chave: Automóvel, Bioradar, Frequency Modulated Continuous Wave, Impulse-Response Ultra-Wide Band, Sinais Vitais

Abstract

Development and validation of a bioradar for automotive mobility systems

In this study, multiple bioradars are studied and tested in an automotive environment, with the objective of making a vital sign detection system that can be used to monitor the Respiratory Rate and Heart Rate of passengers in mobility systems, such as Shared Autonomous Vehicles.

Previous research on this topic is mainly focused on their use in controlled environments, with only a few studies that focus on automotive environments, and only on driver monitoring. Passenger monitoring in an automotive environment is more challenging than in other environments due there being more sources of interference, such as the closed environment and motion of the vehicle, and is also more challenging than driver monitoring, because in that case the bioradar can be placed on or below the steering wheel, reducing the distance to the subject and restricting the detected space to only include the driver.

Three bioradars were tested, the first being a pre-built bioradar with Respiratory Rate and Heart Rate measuring capabilities, and last two being based on commercially available radar modules, one an Impulse-Response Ultra-Wide Band radar and the other a Frequency Modulated Continuous Wave radar, for which multiple variations of vital sign detection software were developed. Tests were made in a van, where the first bioradar was used to record vital sign measurements and the last two were used to record raw data while a contact-based device was used to record ground truth measurements. Afterwards, the developed software was used to measure vital signs based on the recorded raw data of the last two radars, and the vital sign measurement performance of each bioradar and software variation was evaluated by comparing the measurements to the ground truth.

When the vehicle is stationary, the Impulse-Response Ultra-Wide Band radar, when using the loopback filter method, had the best Respiratory Rate measurement performance (6.28 % average Mean Relative Error), and the Frequency Modulated Continuous Wave radar, with settings that provided a higher framerate, and using differential data and phase correction, provided the best Heart Rate measurement performance (3.19 % average Mean Relative Error). When the vehicle is in motion, results are more inconsistent and hard to evaluate. In general, the results suggest that vital sign monitoring using a bioradar is possible in an automotive environment, but requires more research.

Keywords: Automotive, Bioradar, Frequency Modulated Continuous Wave, Impulse-Response Ultra-Wide Band, Vital Signs

Contents

List of Figures

List of Tables

Acronyms

ADC Analog-to-Digital Converter.

DACM Differential and Cross-Multiply.

EM Electromagnetic.

FFT Fast Fourier Transform.

FMCW Frequency Modulated Continuous Wave.

HR Heart Rate.

HRV Heart Rate Variability.

IF Intermediate Frequency.

IR-UWB Impulse-Response Ultra-Wide Band.

MRE Mean Relative Error.

OOI Object of Interest.

PRF Pulse Repetition Frequency.

RR Respiratory Rate.

SAV Shared Autonomous Vehicle.

VCO Voltage Controlled Oscillator.

Chapter 1

Introduction

1.1 Context and Motivation

There has been much interest and research in the area of autonomous vehicles in the past years, and advances in this technology are bringing it closer to the point of fully autonomous, self-driving vehicles. The first form these vehicles will take is likely to be that of Shared Autonomous Vehicles (SAVs) used for mobility services. In fact, many car manufacturers and mobility service companies are conducting research with the goal of creating mobility services based on SAVs [1].

In these vehicles, unlike in current traditional mobility services, there will be no driver present at all times to supervise the state and wellbeing of the passengers, and at times a single passenger might even be traveling alone in an SAV, in which case the passenger will be completely unsupervised. Therefore, it is important that there is a system that is able to monitor the passenger's state, in order to detect sudden illnesses or other relevant changes in the passenger's state so that they can be acted upon in time to avoid or mitigate risks and consequences.

Such a monitoring system would determine the passenger's state based on several of their vital signs. Ideally, the employed vital sign acquisition methods should also be contactless and require minimum to no effort from the passenger so as to not have negative impact on their comfort and experience. The collected data about the passenger's state can also be useful to the service provider, as an indicator of the service's quality, or to the passenger themselves, for other health monitoring purposes. A similar system could also be applied to the driver in traditional vehicles in order to, e.g., determine their workload, which can be a sign of stress or impaired driving capabilities.

Respiratory Rate (RR) and Heart Rate (HR) are two important vital signs of the human body that could

be very useful in a passenger monitoring system. RR can be a strong indicator of serious illnesses, such as cardiac arrest and other events that merit admission to an intensive care unit [2]. HR is also an important vital sign, as it is directly linked to heart diseases [3] and elevated levels of HR can also be indicative of physical stress and high workload.

In order to detect these vital signs in a contactless manner, a bioradar could be used. A bioradar is a radar that is able to detect human presence or measure vital signs, more specifically RR and HR, through the chest movements associated with these physiological functions. These movements are detected at a distance and in some cases can even be measured if the subject is behind a non-metallic barrier [4].

1.2 Objectives

The objective of this study is to develop a contactless passenger RR and HR monitoring system based on a bioradar and implement it in an automotive environment, with the goal of this technology being of use in future automotive mobility systems, such as SAVs. As such, the tasks that must be done in order to reach this objective are as follows:

1. Evaluation of the characteristics and technology of the available bioradars;
2. Development of custom vital sign measurement software for each of the bioradars;
3. Data collection using the bioradars in an automotive environment;
4. Analysis of the collected data;
5. Evaluation of the vital sign measurement performance of each bioradar.

1.3 Dissertation Structure

In Introduction, chapter 1, the motivation, objectives and structure of this dissertation are presented. In Background, chapter 2, necessary information is presented so that the remainder of the dissertation can be better understood. In State of the Art, chapter 3, previous research that has been done in the area of bioradars is presented. In Test Setup, chapter 4, a radar assessment is presented and the used

algorithms and test procedures are described. In Results and Discussion, chapter 5, the results of the previously described tests are presented and analyzed. In Conclusions and Future Work, chapter 6, the conclusions of this thesis are summarized and possible future work is outlined.

Chapter 2

Background

In this chapter a few key concepts related to the research are explained in order to set the context and a basis of information for the rest of the thesis. The addressed topics are human physiology related to the lungs and the heart, radar technology and different types of radar system, as well as descriptions of the devices that are used in this study.

2.1 Cardiac and Respiratory Cycles

In this section the basic aspects of the human lungs and heart are described, as well as the mechanical role of those organs in the respiratory and cardiac cycle. There are three sections, one for the lungs and respiratory cycle, another for the heart and cardiac cycle, and a a section for describing the Zephyr BioHarness, a device used to measure RR and HR in this study.

2.1.1 Lungs and Respiratory Cycle

Lungs are located in the thorax, each of them within a cavity surrounded by a serous membrane called the pleura. As can be seen in Figure 1, the left lung is smaller than the right lung in order to make room for the pericardium, where the heart is. Each lung is composed of smaller units called the lobes, the right lung is composed of three lobes and the left lung of only two [5].

When breathing, the human body uses a series of muscles. Each respiratory cycle begins with the inspiration of air when the lungs expand, lowering the air pressure inside of them which in turn causes

outside air to enter. To achieve the expansion of the lungs, the thoracic cavity itself expands. This expansion is enabled mainly by the diaphragm, which contracts to pull down the bottom of the thoracic cavity, and other muscles that contract to expand the ribcage [6].

Expiration, when not forced, is a passive process, where the muscles used during inspiration relax and the thoracic cavity returns to its relaxed state [7]. When forcefully expiring however, some abdominal muscle pairs are used to contract the thorax. These muscles pull the ribcage down and inwards and push the diaphragm up, contracting the thoracic cavity past its relaxed state, increasing the air pressure inside the lungs and pushing the air out [6].

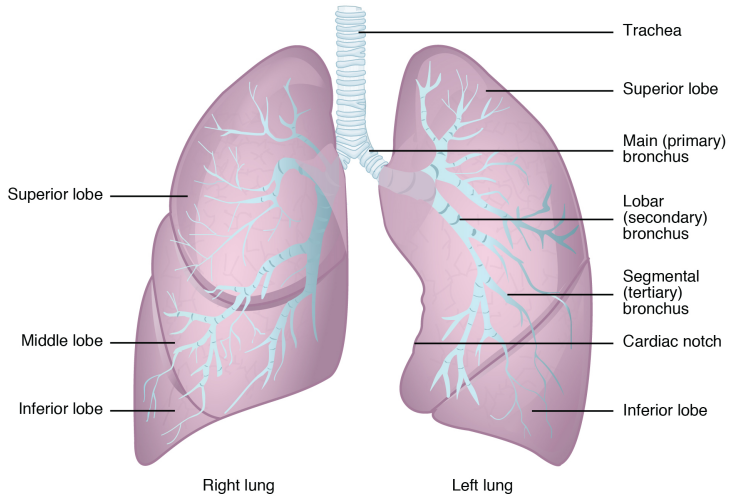

Figure 1: Anatomy of the human lungs. The difference in size and number of lobes can be clearly seen, as well as the airways that reach inside of them [5].

2.1.2 Heart and Cardiac Cycle

In the case of the cardiac cycle, only a single muscle, the heart, is used. It contracts and relaxes periodically to pump blood throughout the human body. The heart is located medially between the lungs separated from other structures by a membrane known as the pericardium.

As can be seen in Figure 2, the heart is composed of four chambers, the left and right ventricles and atria, and four valves, the bicuspid valve, mitral valve, aortic valve and pulmonary valve. The atria are the smaller chambers, located on the upper and broader part of the heart, which is referred to as its base, and the ventricles are the larger chambers, located on the lower and narrower part, also known as the apex. The valves connect different chambers to each other and to the veins and arteries leading to and from the heart [5].

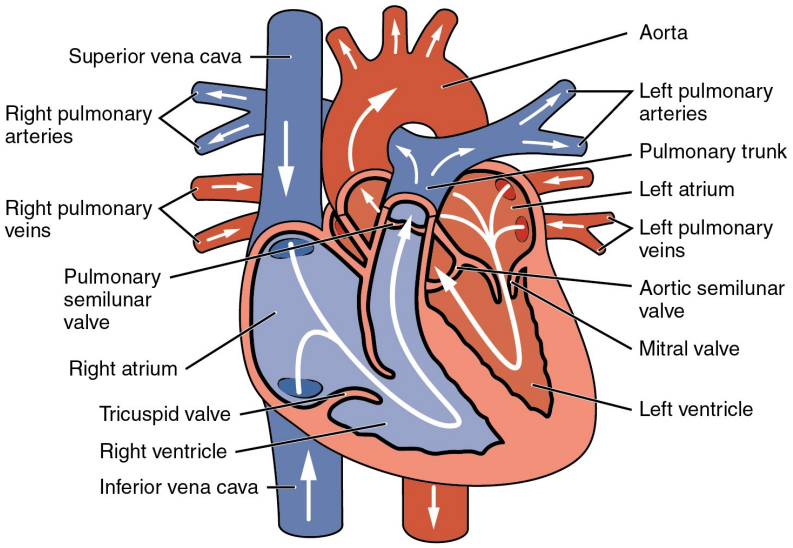

Figure 2: Anatomy of the human heart. The chambers and valves are visible, as well as arrows showing the direction of bloodflow [5].

The cardiac cycle is defined by the contraction and relaxation of the heart chambers and the opening and closing of the heart valves. When an atrium or ventricle are relaxed or relaxing they are said to be in diastole, and when contracted or contracting they are said to be in systole. It is divided into separate phases as the ventricles and atria are in diastole or systole, and the valves open or close due to pressure differentials to block or allow bloodflow [5]. Throughout this cycle the heart contracts and expands, resulting in a cyclical mechanical motion that is repeated for each cardiac cycle.

Even though HR is important, another very common way of identifying heart disease is through Heart Rate Variability (HRV). HRV is the fluctuation in the time intervals between adjacent cardiac cycles, and serves as an indicator of neurocardiac function. A normal human heart does not follow a steady heartbeat rhythm, it naturally has fluctuations in the time between heartbeats, and the presence of pathologies can either accentuate or diminish that variation. There are multiple HRV metrics, associated with different phases of the cardiac cycle and different ways of analyzing the data. HRV metrics are normally extracted from 24-hour data recordings, since an entire day of cardiac activity, including active, resting, and even sleeping times, is better for diagnosis than shorter duration recordings. Nevertheless, HRV measurements based on short duration recordings can also be made, but are more indicative of a subject's immediate state rather than an overview of their cardiac function [8].

2.1.3 Zephyr BioHarness

A contact-based vital sign measuring device, the Zephyr BioHarness, was used to provide ground truth measurements in this study. This device is based on a chest strap, that is worn by the subject below the sternum, which contains a pressure sensor to detect breathing through the expansion of the ribcage and electrode pads that detect the subject's heartbeat. The sensors' outputs are analyzed by a module that connects to the strap, converts the data into RR and HR measurements expressed in beats per minute and breaths per minute, respectively, and sends the measurements to a computer via Bluetooth. The measurements can then be saved in text files for later analysis.

This device has been proven to be able to measure both RR and HR with high reliability for healthy males and females when they are at rest, during physical activity and during recovery from physical activity [9] [10].

2.2 Radar Technology

This section starts with an overview of the basic principles of radar technology, followed by a more detailed look into a few different types of radar, more specifically Impulse-Response Ultra-Wide Band (IR-UWB) radar and Frequency Modulated Continuous Wave (FMCW) radar, and finally a section where the different radar systems used in this study are described.

2.2.1 Basic Principles

A radar is a detection system based on radio frequency Electromagnetic (EM) waves. The details of the operation and components of radar systems differ on a case to case basis, however, the core principles remain the same, and some subsystems are always present, specifically the transmitter, antenna, receiver and signal processor [11].

In broad terms, radars function by transmitting EM waves, that are modulated by the transmitter, through the antenna to their surroundings. These waves are then reflected by objects in the environment, including, not only the Object of Interest (OOI), but also other objects. The reflected wave, or echo, then returns to the radar's antenna, where it is captured and sent to the receiver, an analog circuit that amplifies

the received signal, and, if necessary, demodulates and/or converts it using an Analog-to-Digital Converter (ADC) before sending it the signal processor. Finally, the signal processor is where the signal is analyzed in order to extract the desired information from the OOI's [11]. This analysis may include many different techniques that depend on the type of radar and the type of information that is being sought. A simplified diagram depicting this process can be observed in Figure 3.

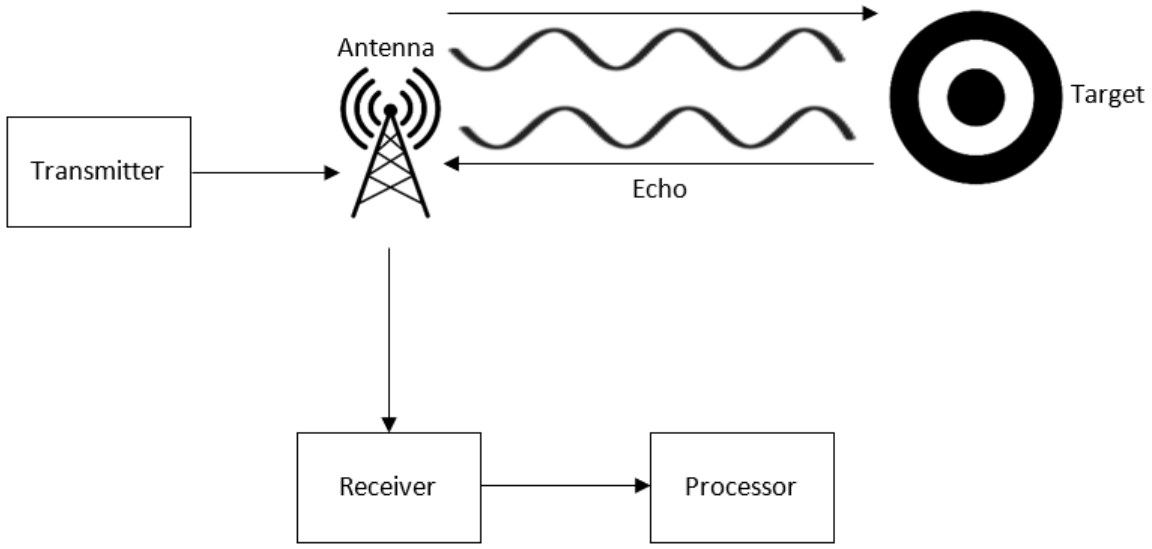

Figure 3: Simplified graphic representation of the operation of a generic radar.

The presence of objects other than the OOI causes interference known as clutter, which is the main type of interference in radar systems. There are, however, more sources of interference, such as internal and external electronic noise, and EM waves from sources other than the radar system. The detection of the OOI despite the presence of interference is the main function of the signal processor, and one of the main challenges to overcome in radar system design [11].

2.2.2 Types of Radar Technology

As previously mentioned, radar systems can differ from each other in many ways, however, the main defining characteristic of a radar system is the waveform that it transmits. The following subsections will provide background on how some types of radars function, specifically IR-UWB radars and FMCW radars, as these are the types of radar that are used in this study.

2.2.2.1 Impulse Response Ultra-Wide Band Radar

In an IR-UWB radar, the transmitted wave is a short duration pulse, similar to the one shown in Figure 4. This pulse travels to the environment, where it is reflected and sent back to the radar system, where it is received.

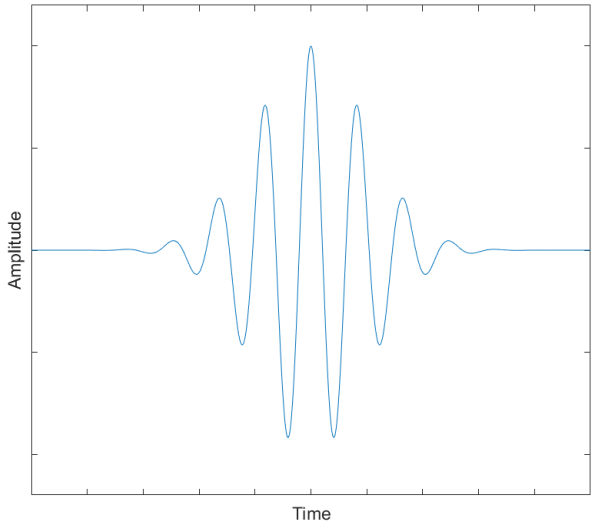

Figure 4: Example of an EM pulse generated by the transmitter of an IR-UWB radar.

Since the pulse travels at a known speed, the speed of light, it is possible to determine the distance traveled by the pulse by multiplying this speed with the pulse's travel time. Because the pulse covers this distance twice, once when going from radar to OOI, and again in the return trip, this corresponds to twice the distance from radar to OOI. Taking this into account, the formula used to calculate the distance to OOI can be seen in Equation 2.1, where d is the distance to the OOI, Δt is the pulse's travel time, and c is the speed of light.

$$d = \frac{\Delta t \cdot c}{2} \tag{2.1}$$

In this type of radar, the receiver samples the received EM wave at a very high rate in the moments after sending a pulse, generating a signal known as a frame, an example of which can be seen in Figure 5. Each sample in a frame corresponds to a different time of sampling, and, consequently, to a different travel time and range to a reflecting surface. A frame is generated for each pulse sent by the radar, and these frames are the data that must be analyzed by the processor in order to extract relevant data.

In order to analyze the radar data, frames that are collected in succession can be organized in what will be referred to as a range-time matrix. A range-time matrix is two-dimensional, one dimension corresponding to the number of the frame, and another to the number of the sample. As can be seen in Figure

6, each line corresponds to a single frame, such as the one in Figure 5, and each column to a sample. Assuming that frames are collected at a constant rate, the number of the frame is proportional to the time of recording, also known as slow time. Similarly, the number of the sample also corresponds to a particular elapsed time within each frame, which is known as fast time. Because fast time is the travel time of the signal, this can also be converted to detected range instead.

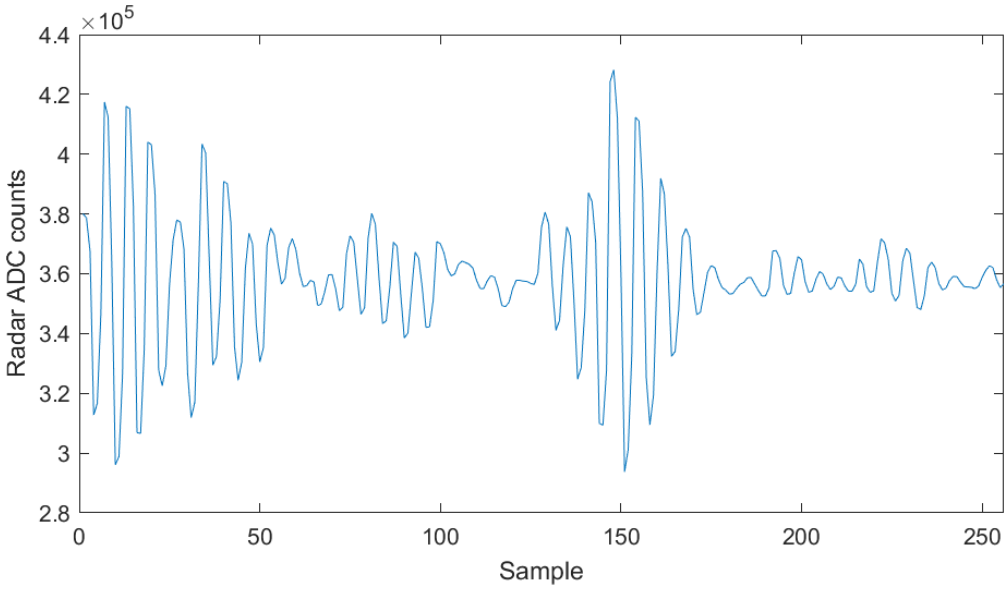

Figure 5: Example of a frame generated by an IR-UWB radar.

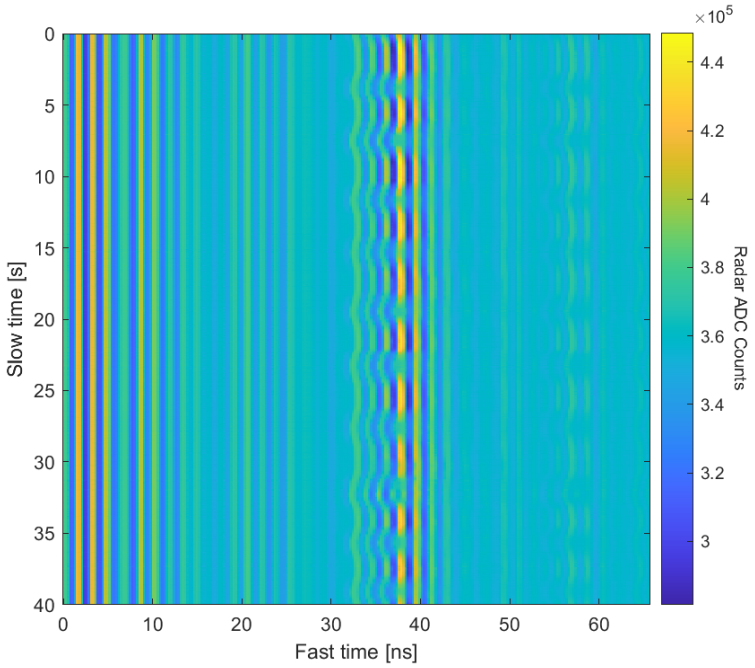

Figure 6: Example of a range-time matrix.

2.2.2.2 Frequency Modulated Continuous Wave Radar

FMCW radars are more complex than IR-UWB radars both in transmitted waveform and output data. Instead of pulses, the transmitters of FMCW radars generate chirps, waves that are modulated in frequency over time [12]. Chirps can have a multitude of shapes, the most common and simple of these being the sawtooth. In this chirp shape, the frequency of the transmitted wave is modulated to increase or decrease linearly over the duration of the chirp, as can be seen in Figure 7a, resulting in a signal similar to the one in Figure 7b.

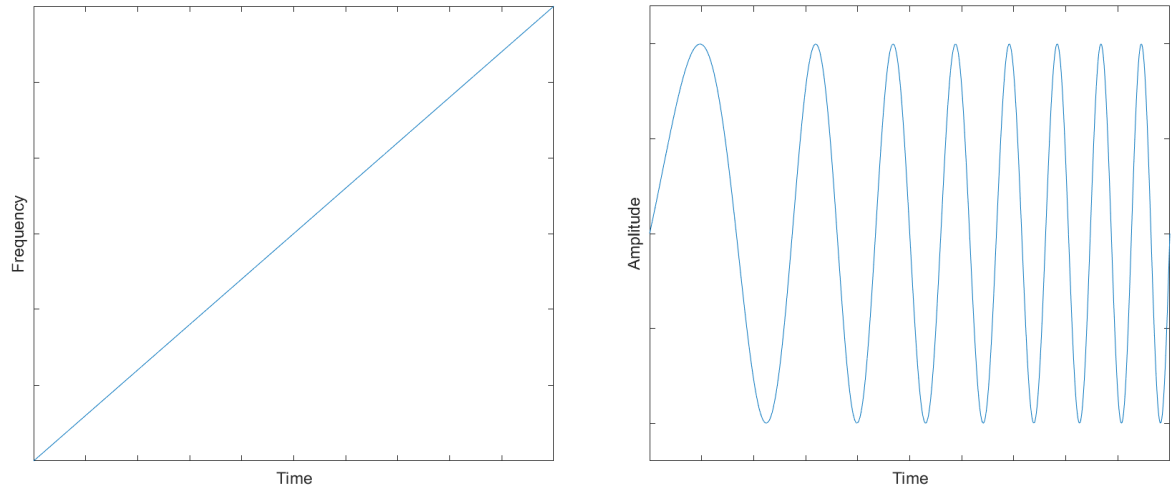

Figure 7: Sawtooth chirp from an FMCW radar: a) Frequency over time; b) Signal over time.

The radar transmits chirps to the environment in succession, where they are reflected back to the radar and captured by the receiving antenna. Because each chirp is modulated in frequency according to a know pattern, it is possible to utilize frequency as a timestamp to know when each portion of the chirp that is reflected back to the radar was sent [12]. In the case of linear chirp shapes, such as sawtooth, the difference in frequency between the received signal and the signal that is being sent at the moment of reception, called the beat frequency, is directly proportional to the travel time of the EM wave, and, as such, directly proportional to the range of the reflecting object.

In order to output this information, the radar's receiver generates a signal containing frequency components corresponding to the beat frequencies of all the detected objects. This is called the beat signal or Intermediate Frequency (IF) signal, and it is generated by a mixer that demodulates the received signal using the current transmitted signal as a reference. In short, it is as if the received signal was an FM radio signal and is being demodulated as if the transmitted signal was the carrier signal.

In Figure 8, the relation between the transmitted signal, received signal and beat frequency when a

single, stationary target is detected and a sawtooth chirp is being used can be seen. Because the target is stationary, the received signal is the same as the transmitted signal, only delayed in time, and because the chirp shape is linear, the difference in frequency between the two is constant, resulting in a constant beat frequency. In a real-world application, there would be objects detected at multiple ranges, resulting in multiple beat frequencies, and the beat signal would have a frequency component for each range with detections.

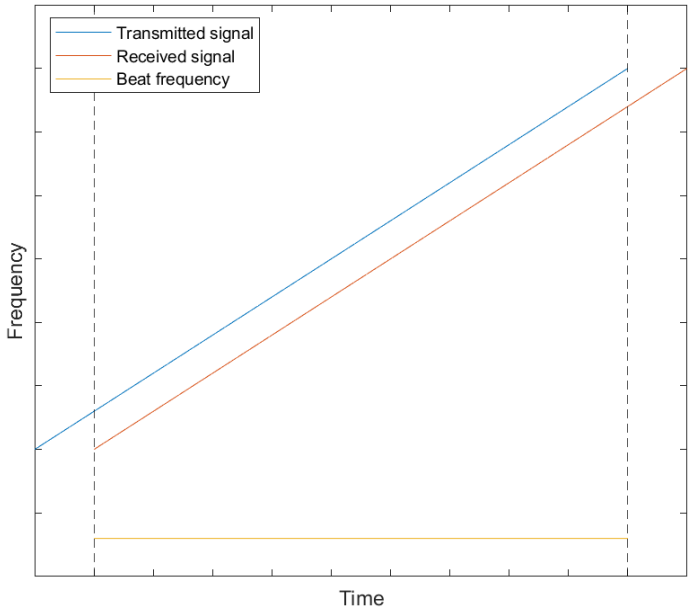

Figure 8: Relation between transmitted signal, received signal and beat frequency when a single, stationary target is detected and a sawtooth chirp is being used.

In mathematical terms, the beat signal for a single beat frequency can be seen in Equation 2.2, where A is the amplitude of the signal, which is affected by a multitude of factors, $\gamma = \frac{BW}{T_{Chirp}}$, BW being the transmitted bandwidth i.e., the difference the maximum and minimum transmitted frequencies, and T_{Chirp} being the chirp duration, R is the target range, f_c is the center frequency of the chirp and c is the speed of light [13].

$$s_b(t) = A \cdot \exp\left(j\left(\frac{4\pi\gamma Rt}{c} + \frac{4\pi f_c R}{c} + \frac{4\pi\gamma R^2}{c^2}\right)\right) \tag{2.2}$$

Considering that the beat frequency, f_b, can be defined using Equation 2.3, that the phase of the beat frequency component, ϕ_b, can be defined using Equation 2.4 and that the final term represents residual video phase and is negligible due to being proportional to $1/c^2$, Equation 2.2 can then be simplified into Equation 2.5

$$f_b = 2\gamma R/c \tag{2.3}$$

$$\phi_b = 4\pi f_c R/c \tag{2.4}$$

$$s_b(t) = A \cdot \exp(j(2\pi f_b t + \phi_b)) \tag{2.5}$$

The beat signal is then modulated into an I/Q signal pair, a type of modulation that allows for phase information to be transmitted on to the processor. This is done by decomposing the beat signal into two channels, the I-channel and the Q-channel. Considering that a sinusoidal signal can be defined as $S(t) = cos(\omega t + \varphi)$, the mathematical decomposition of a sinusoidal into an I/Q signal pair can be seen in Equation 2.6.

$$\begin{aligned} S(t) &= cos(\omega t + \varphi) && \Leftrightarrow \\ &= cos(\varphi) \cdot cos(\omega t) - sin(\varphi) \cdot sin(\omega t) && \Leftrightarrow \\ &= cos(\varphi) \cdot cos(\omega t) + sin(\varphi) \cdot cos(\omega t + \pi/2) \end{aligned} \tag{2.6}$$

The two terms can be split into two different sinusoidal signals, expressed in Equation 2.7.

$$I_S(t) = cos(\varphi) \cdot cos(\omega t) \quad , \quad Q_S(t) = sin(\varphi) \cdot cos(\omega t + \pi/2) \tag{2.7}$$

Therefore, the original sinusoidal signal can be modulated into an I/Q signal pair, with the Q channel, also known as the in-quadrature channel, always having a $\frac{\pi}{2}$ phase in relation to the I-channel. The amplitudes of both these channels are modulated in accordance to the phase of the original signal, and this phase can be reconstructed by adding both channels. A graphic example of this process can be seen in Figure 9, where the sum of a pair of amplitude modulated I/Q waves reconstructs a sinusoidal wave with amplitude of 1 and phase of $\frac{\pi}{3}$ radians.

Each beat signal is the sum of all its beat frequencies, or, in other words, it is the sum of multiple sinusoidal signals. The I/Q signal pair of a signal with multiple frequency components is the sum of the I/Q signal pairs of each component. Therefore an I/Q signal pair can be generated for a beat signal, and the frequency and phase information of each beat frequency can be passed on to the processor.

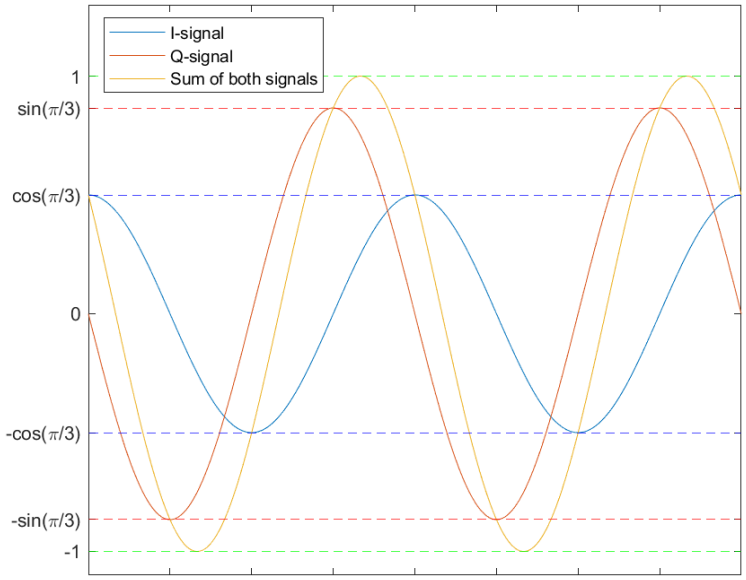

Figure 9: Example of I/Q modulation for a sinusoidal wave with amplitude of 1 and phase of $\frac{\pi}{3}$ radians.

When processing the beat signal that originates from an FMCW radar, to determine at what ranges objects were detected, it is necessary to perform a Fast Fourier Transform (FFT). This separates the frequency components of the beat signal, each bin of the FFT corresponding to a different range bin. Because of this, the process is called a range-FFT. In the case of sawtooth shaped chirps, based on Equation 2.3, the range R of an object can be determined based on it's beat frequency using Equation 2.8 [13].

$$R = \frac{1}{2} \cdot \frac{f_b}{BW} \cdot T_{Chirp} \cdot c \tag{2.8}$$

As demonstrated, through the range-FFT it is possible to separate the beat frequencies present in the beat signal and attribute them a range, however, the range resolution that results from this is limited by the resolution of the FFT. In order to achieve greater range resolution within a specific frequency bin of the range-FFT, the phase data of the corresponding frequency bin can be analyzed. Based on Equation 2.4, range can also be determined using Equation 2.9. This greatly increases the range resolution capabilities of FMCW radars, and is possible due to I/Q modulation retaining the phase information of the signal, which other modulation techniques might not be able to do [13].

$$R = \frac{\phi_b}{4\pi f_c} \cdot c \tag{2.9}$$

While the first of these two range measurement techniques provides an absolute measurement of the OOI's distance to the radar by calculating the range of a specific frequency bin, the second can only be used to detect movement within a specific range bin, because, depending on the resolution of the range-FFT, a

single range bin can span multiple f_c wavelengths, and, therefore, a single phase value could correspond to multiple different ranges within a range bin. Because of this, this technique can only be employed after the first, and can only be used as a way to detect an OOI's movement over multiple chirps, and in relation to a reference range.

2.2.3 Available Radar Systems

In this subsection, the used radar systems will be described, as well as how they are operated. The radar systems that are used in this study are the SensorLogic Ancho Radar Development Kit (Figure 10a), the SensorLogic Onza Radar Development Kit (Figure 10b), the Xandar Kardian Presence Detection with Vital Sign Monitoring bioradar (Figure 10c) and the Staal Technologies RIC60A Radar Development Kit (Figure 10d).

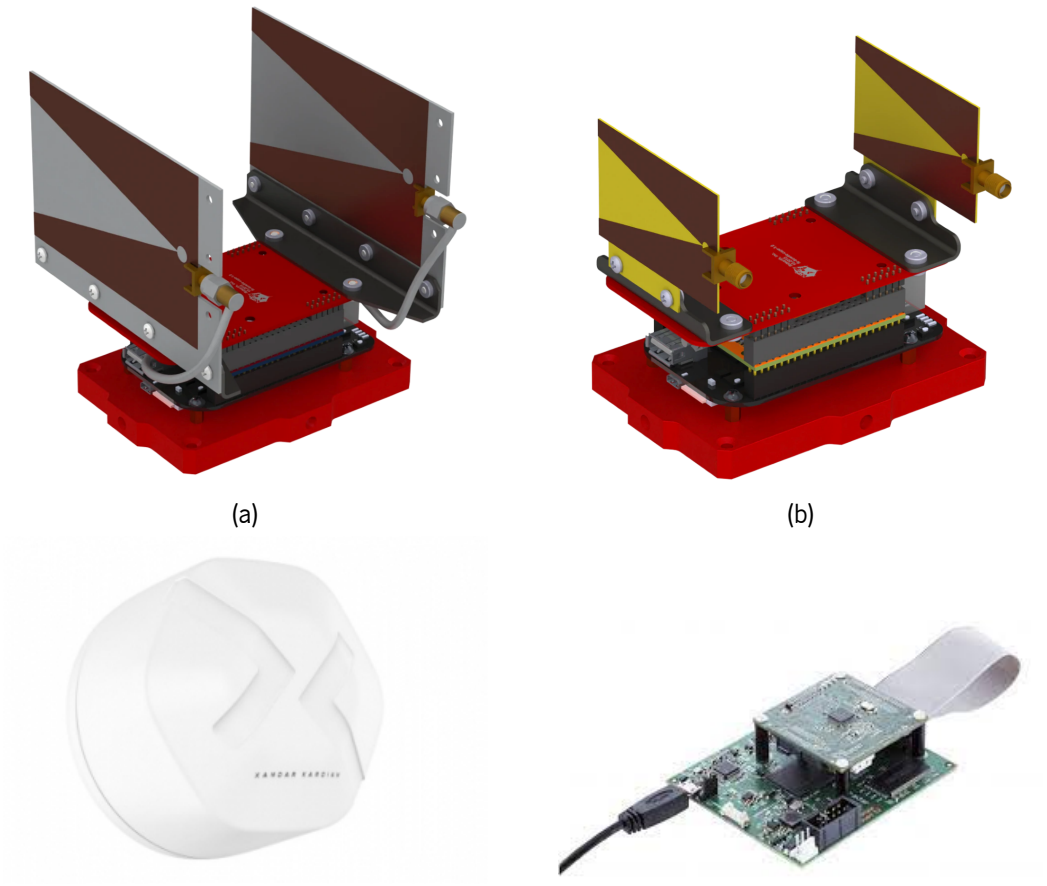

(a) (b)

(c) (d)

Figure 10: Radar modules used in this study: a) Ancho Radar Module; b) Onza Radar Module; c) Xandar Kardian Presence Detection and Vital Sign Monitoring Radar; d) RIC60A Radar Module.

2.2.3.1 SensorLogic Ancho Radar Development Kit

The SensorLogic Ancho Radar Development Kit includes the Ancho radar module, depicted in Figure 10a, and the Salsa Software Suite. The radar module is based on the XeThru X2 impulse radar transceiver, a commercial radar chip that allows for IR-UWB radar sensing whose main characteristics are detailed in Table 1. The chip is controlled through a BeagleBone Black microcontroller, that is loaded with software provided by the manufacturer and connects to a computer via USB, where it can be controlled using software from the Salsa Software Suite. The Salsa Software Suite is a set of packages and resources to utilize with the Ancho radar module. The most important of these, for this study, is a MATLAB package that includes a radar wrapper that allows the user to connect the radar to the computer, manage the radar's settings and receive data.

Table 1: Characteristics of the XeThru X2 impulse radar transceiver.

Output pulse center frequency	5.3 - 8.8 GHz
Samples per frame	256
Sampling rate	39 GHz
Detection range	0.98 m
Range resolution	3.8 mm
Pulse Repetition Frequency	100 MHz

The XeThru X2 chip samples the received signal using a set of 256 parallel samplers, that each trigger at a different time interval after the signal is sent, allowing for a fast sampling of the received EM wave. After that, the sampled signal is sent to the ADC, in repeating pulses at a constant Pulse Repetition Frequency (PRF). The ADC converts each sample by sweeping the possible values from the ADC minimum to the ADC maximum, and then on the opposite direction in the next iteration, and so on. For each step, the value of the pulse is compared to the current ADC value, and if it is still too high or low, the value is incremented or reduced by the ADC step value. Alternatively, multiple pulses can be read for each step, increasing the accuracy of the ADC. This process is simultaneous for every sample of the signal. The ADC minimum, maximum, step, number of pulses per step and number of iterations can all be set using the MATLAB wrapper. A higher number of pulses per step, iterations, and reduced ADC step increases the quality of the data, however, it also increases the time it takes to convert each frame, reducing the amount of frames the radar can capture, convert and send each second. Therefore, a compromise must be made between signal quality and framerate. The delay before the samplers start triggering can also be set, which can be

used to move the detected range closer or further away from the radar. When all the settings are defined, the wrapper is used to make the radar output data by asking for each frame individually.

2.2.3.2 SensorLogic Onza Radar Development Kit

The SensorLogic Onza Radar Development Kit is very similar to the Ancho kit, but with a Onza radar module instead, which is depicted in Figure 10b. This module is similar to the Ancho module in every way, except in that it uses a XeThru X4 impulse radar transceiver instead. This chip is similar to the XeThru X2 chip in the way it operates, but has different characteristics, that can be seen in Table 2. This radar chip has more samples per frame and reduced sampling rate. This increases its range significantly, but decreases its range resolution too. This chip's ADC works in the same way as the ADC of the previous chip, however, the PRF is significantly reduced, slowing down the process of conversion, which impacts the framerate of the radar module.

Table 2: Characteristics of the XeThru X4 impulse radar transceiver.

Output pulse center frequency	7.29 - 8.75 GHz
Samples per frame	1536
Sampling rate	23.328 GHz
Detection range	9.87 m
Range resolution	6.4 mm
Pulse Repetition Frequency	40.5 MHz

2.2.3.3 Xandar Kardian Presence Detection with Vital Sign Monitoring

The Xandar Kardian Presence Detection with Vital Sign Monitoring sensor, depicted in Figure 10c, is a bioradar that is able to detect human presence through movement detection and measure RR and HR after presence has been detected. The bioradar is based on Novelda's X4M02, a IR-UWB radar module, and an integrated microcontroller that processes the radar data. The module connects to a computer via USB or Wi-Fi, where a software application is used to change radar settings and receive data. The specific radar and software that was used for testing was customized by the manufacturer for vital sign detection in an automotive environment, and is therefore different in some ways from the commercially available version of the bioradar.

To operate the radar, after connection has been made to the computer, the application, that can be seen in Figure 11, must be opened and the correct serial port selected. After that, some radar settings

can be changed before the calibration process is conducted. Calibration starts after a delay defined by the user when the auto calibration button is pressed on the application. During calibration, the detection area of the radar should be empty of people, so that the environment can be sensed and that data later used in clutter removal to improve the performance of the bioradar.

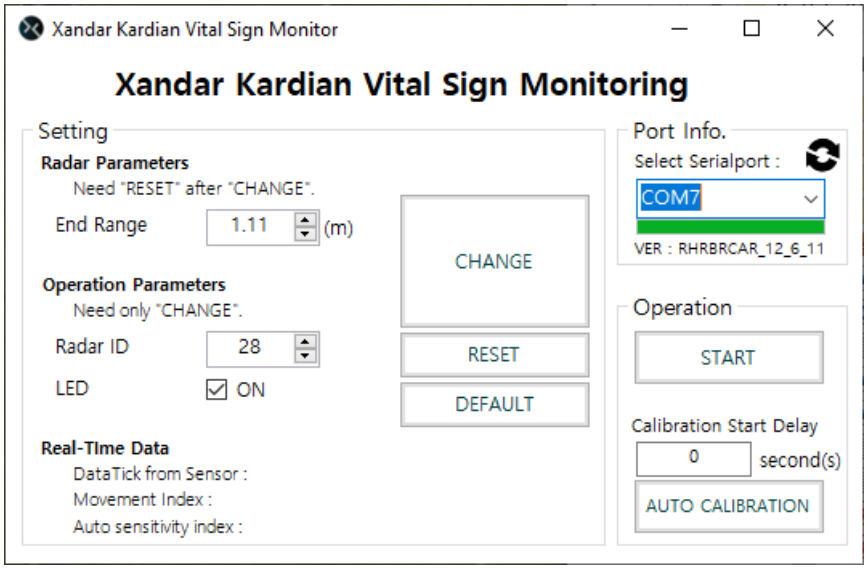

Figure 11: Xandar Kardian Presence Detection with Vital Sign Monitoring application main window.

To access the current RR and HR measurements, the start button must be clicked, which opens a new window that can be seen in Figure 12. In this window the current measured RR and HR, a reliability metric for both vital signs and a movement metric are displayed. This version of the bioradar outputs constant RR and HR measurements, however, the reliability metric only increases past 0 if the movement metric is at 100, meaning that the radar considers that there is no movement other than breathing and heartbeat, and this RR and HR measurements can be performed. After that, the reliability metric can start increasing if the system is confident in the measurements, but will decrease again if movement is detected or the data is considered to be poor. Because of this, RR and HR measurements should only be taken into account if their respective reliability value is high. If the radar detects no movement at all, then the space is considered to be vacant and no vital sign measurements are taken. All the received data, including vital sign measurements and reliability metrics, is stored in a text file for later analysis. The algorithms used by the bioradar to detect movement, perform measurements and calculate reliability are entirely unknown, as they are not disclosed by the manufacturer and the system is completely integrated within the radar module, connecting to the computer only to send data and receive instructions.

Figure 12: Xandar Kardian Presence Detection with Vital Sign Monitoring application measuring vital signs.

2.2.3.4 Staal Technologies RIC60A Radar Development Kit

The Staal Technologies RIC60A Radar Development Kit, depicted in Figure 10d, is a radar module that includes the Omniradar RIC60A radar chip. This module is capable of operating in FMCW or Doppler mode, includes one transmitting and two receiving antennas, is able to transmit EM waves in the 57 to 64 GHz band and its internal ADC is able to convert the IF signal with a sampling rate of 25 MHz. The radar module connects to the computer through USB, and is controlled using MATLAB. Radar settings are configured by sending a character string to the radar using a MATLAB command. The string contains the radar settings and is generated using a software application provided by the manufacturer that outputs the correct string after selecting the desired settings.

The frequency of the signal transmitted by the radar is defined by the voltage that is fed to the Voltage Controlled Oscillator (VCO), this voltage can range from 0 to 3 V, 0 V being the start of the band, i.e., 57 GHz, and 3 V the end, i.e., 64 GHz. This voltage is set by the user using a MATLAB command that can have either a vector or a scalar as an argument. If a vector is set, that will be the VCO voltage over time for a single chirp in FMCW mode, if a scalar is set, that will be the voltage fed to the VCO continuously for Doppler mode. The chirp time is set separately using a different command. After all is set, the user can obtain chirps by using another command, and multiple chirps can be requested at the same time, in which case they are done in succession.

As previously said, the frequency transmitted by the radar is related to the VCO voltage, however, this is not a linear relation in practice due to small imperfections in the hardware, and therefore the relation between VCO voltage and transmitted frequency, called the frequency curve, must be first determined before the radar can be used. This is a process that can also be done using a MATLAB script provided by the manufacturer. After this, it is possible to use the frequency curve to generate a VCO voltage vector

that, in practice, makes the radar transmit the desired chirp shape.

Chapter 3

State of the Art

In this chapter, other work in the area of vital sign detection will be discussed, with focus on studies made using IR-UWB or FMCW radars, because these are the types of radar used in this study. This chapter is split into three sections, one for the concept of chest movement signal, and two for the state of the art research that has been done for each type of radar explored in the previous chapter.

3.1 Chest Movement Signal

The chest movement signal is the signal that conveys the distance between the surface of the subject's chest and the radar over time. This distance is affected by the subject's respiration and heartbeat, each of these adding a periodic component to the signal with different frequencies, f_r and f_h, and different amplitudes, A_r and A_h, the respiration component having a much larger amplitude than the heart beat component. Therefore, the chest movement signal $s(t)$ of a stationary subject with a base distance d_0 to the radar can be modeled using Equation 3.1 [14].

$$s(t) = d_0 + A_r \cdot sin(2\pi f_r t) + A_h \cdot sin(2\pi f_h t) \tag{3.1}$$

This model, however, is very simplified, and does not take into account a multitude of factors, such as human respiration and heart beat frequency and amplitude being dynamic and varying between cycles, and the baseline distance to the radar changing over time as the subject moves their torso, which is a major obstacle to overcome and the reason why the vital sign detection algorithms using bioradars, in general, can only measure the vital signs of stationary subjects. Nevertheless, it is a suitable starting

point.

For a bioradar to measure a subject's respiratory rate or heart rate, it must be capable of measuring the subject's chest movement signal, and different types of bioradar achieve this through different means, due to the data that they generate. Different techniques can also be applied in order to isolate and filter this signal.

3.2 IR-UWB Radar

Many studies have been made using this type of radar to measure vital signs based on chest movement, some even in an automotive environment. Lee *et al.* [15] use this type of radar to attempt to measure the HR and HRV of a newborn in a neonatal intensive care unit. Rong *et al.* [14] propose a method for HR estimation in stationary subjects. Yin *et al.* [16] propose a method to measure HR that includes body movement compensation, so that the vital sign can be measured even if the subject is in motion. Lee *et al.* [17] propose a method to measure HR and HRV with the purpose of detecting arrhythmia using an IR-UWB radar, and validate it using a large number of test subjects including healthy volunteers and patients with atrial fibrillation. Pittella *et al.* [18] use a wearable radar of this kind to measure RR and HR. Ding *et al.* [19] propose a method to simultaneously measure the RR of multiple subjects using a single IR-UWB radar. Khan *et al.* [20] also propose an algorithm to measure RR and HR in a subject, with a body movement detection feature. Yang *et al.* [21] propose a method of utilizing an IR-UWB radar to measure the RR of a subject inside a vehicle, and test multiple positions for the radar. And finally, Leem *et al.* [22] utilize a radar of this kind to measure RR and HR of a driver and detect mobile phone usage while driving. Although these studies measure vital signs by evaluating the subject's chest, other methods have been developed to measure HR based on the movement of other body parts, such as the neck or the upper arm.

The employed algorithms differ on the exact methods used to arrive at the vital sign measurements, but all share similar phases, namely, chest movement signal extraction, which includes clutter removal and range detection, and vital sign extraction.

3.2.1 Chest Movement Signal Extraction

Clutter removal is important to remove unwanted interference that could impact the vital sign measurements. As there are multiple types of clutter, such as static clutter from environment or clutter from moving objects, there are also multiple techniques that are employed to minimize it. Static background clutter is caused by static objects in the environment that reflect the radar pulses and cause clutter that is constant or nearly constant throughout all the detected frames. To remove this kind of clutter, in some studies the average of each column in the range-time matrix is subtracted from all the points in that column, a technique called background subtraction [15] [19]. Other studies use a loopback filter, which, for each frame, subtracts static background clutter based on the formula in Equation 3.2, where r_k is the k^{th} received frame, c_k is the clutter of the k^{th} received frame, y_k is the k^{th} frame after clutter is removed and α is a weighting constant. In comparison to the background subtraction method, this method has the advantage of being able to compensate slow changes in the profile of the static background clutter [16] [17] [20] [22]. One study also utilizes the Principal Component Analysis method [18].

$$\begin{aligned} c_k(t) &= \alpha \cdot c_{k-1}(t) + (1-\alpha) \cdot r_k(t) \\ y_k(t) &= r_k(t) - c_k(t) \end{aligned} \tag{3.2}$$

Although static background clutter is one of the main sources of noise, there are more sources of noise and interference. As such, some studies employ further filtering to remove the remaining noise. Some of the employed techniques are wavelet-based methods and Kalman filtering [16] [20].

Range detection is necessary in any vital sign detection algorithm using this kind of radar in order to know from which column of the range-time matrix should the chest movement signal be extracted. Although it is a relatively simple phase of the process, a few different techniques are applied, such as determining which range has the most variance [19] [20] or finding the range with the largest spectral component after clutter removal [18].

After subject range has been determined, the chest movement signal is extracted from the column of the range-time matrix that corresponds to the subject range. Some studies, however, instead of assuming that the subject is stationary for the purposes of measuring vital signs, use algorithms to compensate for body motion, and therefore analyze more than a single range for vital sign measurements and reconstruct the chest movement signal using information from multiple ranges [16] [22].

3.2.2 Vital Sign Extraction

Finally, the vital signs must be measured based on the extracted chest movement signal. An FFT of the chest movement signal results, according to Rong *et al.* [14], and assuming the chest movement signal of Equation 3.1, in a spectrum that contains the frequency components of respiratory rate, heart rate, and their corresponding harmonics. This is the basis of some of the vital sign detection methods in literature, where the FFT of the chest movement signal for a certain period of time is computed and the greatest frequency component inside the limits of human RR/HR is the measured RR/HR, respectively, for that period of time [14] [21] [22]. Another common and simple method is peak detection, where the peaks of the chest movement signal are detected and counted. Given that each peak corresponds to a single respiratory cycle or cardiac cycle, it is possible to use this technique to count the number of cycles in a period of time, which then allows the calculation of RR or HR. This technique is usually applied after filtering the chest movement signal to exclude signal components that could introduce peaks to the signal that are not related to the measured vital sign [15] [17] [21]. This technique, when applied to HR, has the advantage of allowing the measurement of HRV.

Besides these simpler methods, some studies employed more complex algorithms for this phase of the vital sign detection process. Pittella *et al.* [18] note that the strong harmonics of the RR component of the chest movement signal are often inside the limits of HR, and can have amplitudes greater than the HR component, giving way to wrong measurements. Therefore, RR is detected first using the FFT technique described above, and then a custom filter is generated to filter the respiration harmonics out of the signal's spectrum. This filtered spectrum is then analyzed to determine the HR. However, this technique has the issue of not measuring HR properly if the HR frequency is near one of the respiration harmonics, as then the filter also suppresses this component of the signal.

Khan *et al.* [20] employ a method that utilizes data from multiple windows of time of the chest movement signal to determine HR. For each window of time, the FFT of the chest movement signal is computed, and peaks in the spectra within the interval for human HR are detected and the frequency at which they appear recorded. After a predetermined number of iterations, the frequency that registered the most peaks is considered to be the HR. However, this method is very sensitive to respiration harmonics, therefore peaks in frequencies that correspond to the harmonics of the RR for each spectrum are ignored. The major difference between this method and previously mentioned methods is that rather than using amplitude to determine which of the peaks within the HR limits corresponds to HR, the number of appearances of the peaks is used. This reduces the frequency of outliers caused by wrong measurements and increases the

stability of HR measurements.

Some other studies utilize different complex methods to separate, from the chest movement signal, the frequency components of RR and HR. Ding *et al.* [19] use a method called Variational Mode Decomposition to separate the chest movement signal into modes. Because in their study the chest movement signal includes the chest movements of multiple subjects, the objective is to separate the RR components of different subjects into different modes, and identify which modes contain RR components. Afterwards, the Hilbert transform of relevant modes is computed, which provides instantaneous measurements of the frequency of each mode, which translates to instantaneous measurements of each subject's RR over the analyzed time frame. Yin *et al.* [16] utilizes a method called Variational Nonlinear Chirp Mode Decomposition that also separates the signal into modes and also allows instantaneous measurements of RR and HR over the analyzed time period.

3.3 FMCW Radar

This type of radar has also been used in multiple studies to measure vital signs of subjects in controlled environments. Some of the employed techniques are similar to the ones used with IR-UWB radars. However, because of the differences between the radar types, some changes are made to better exploit the advantages of this kind of radar technology. Unlike for the previously discussed type of radar, no studies have been made in automotive environments. Arsalan *et al.* [23] utilize this type of radar and adaptive filtering of the signal to measure the HR of stationary subjects. Antolinos *et al.* [13] utilize one of these radars to separate and acquire the chest movement signals corresponding to respiration and heartbeat of a single or multiple subjects simultaneously. Sun *et al.* [24] propose a method that utilizes data from multiple chirps for each datapoint and signals from multiple ranges to estimate the HR of a subject. Wang *et al.* [25] propose two separate algorithms for respiration and heartbeat signal separation and reconstruction and compare their performance at measuring RR and HR with the conventional FFT-based method. Alizadeh *et al.* [26] propose a method to solve one of this type of radar's problems in signal processing, which is phase discontinuity. Fang *et al.* [27] utilize a FMCW radar to measure the RR and HR of multiple subjects at different ranges simultaneously. Ahmad *et al.* [28] utilize a FMCW radar with multiple transmitting and receiving antennas to measure the vital signs of multiple subjects in different directions simultaneously. Zhang *et al.* [29] use an FMCW radar to measure the RR and HR of a single subject, with an algorithm that aims to improve the separation between the HR component of the chest

movement signal and the harmonics caused by the respiration component.

As previously mentioned, some of the techniques utilized for vital sign measurement with radars of this type are similar to the techniques used for IR-UWB radars, and although changes must be made to accommodate for the differences between the two, the general process remains the same, with the same phases of chest movement signal extraction, including clutter removal and range detection, and vital sign extraction.

3.3.1 Chest Movement Signal Extraction

In the studies conducted using IR-UWB radars, clutter removal was done before range detection. However, in studies made using FMCW radar, range detection usually comes first, because clutter removal is usually done within the desired range bin only. The first step in range detection is always to compute the range-FFT of each chirp that is being analyzed, after that, different studies use different methods to determine in which range bin the subject is present. In some studies, because the distance between subject and radar is known, only a predefined set of range bins is analyzed, and an automatic range detection algorithm is not used [24] [26]. In the studies that did use a form of automatic range detection, it is usually based on determining which range bin shows the strongest reflection throughout the analyzed chirps, sometimes coupled with a form of verification that utilizes a variance threshold to make sure that the detection is not a static object from the environment [25] [23] [27]. Ahmad *et al.* [28], due to the nature of trying to measure vital signals from multiple subjects in multiple directions, utilize a more complex algorithm to detect objects in space, followed by a variance threshold to determine which of the objects are subjects.

An important concept in FMCW radar sensing is the problem of phase ambiguity. As mentioned in the previous section, the range resolution of an FCMW radar can be enhanced through the use of phase analysis, where phase is normally determined using the arctangent function, the formula being $\phi_b[n] = tan^{-1}(Q[n]/I[n])$, where $Q[n]$ and $I[n]$ are the amplitudes of the analyzed frequency bin of the FFTs of the Q and I signals for each chirp n. This analysis, however, is limited by the wavelength of the center frequency f_c in Equation 2.9, because if the movement range of the chest movement signal is larger than a wavelength, the phase can go under $-\pi$ or over π, causing it to wrap around to the other extreme and cause discontinuities. Because the center frequency tends to be high and, by consequence, the wavelength short, it is important to use a phase unwrapping method to eliminate these discontinuities. The first method is the Differential and Cross-Multiply (DACM) algorithm, which turns the arctangent function

into a derivative function, as can be seen in Equation 3.3 [25]. This method is utilized in some of the studies using this type of radar [13] [25].

$$\frac{d}{dn}\phi_b[n] = \frac{d}{dn}tan^{-1}\left(\frac{Q[n]}{I[n]}\right) = \frac{I[n]Q'[n] - I'[n]Q[n]}{I[n]^2 + Q[n]^2} \tag{3.3}$$

Because $Q[n]$ and $I[n]$ are discrete signals, Equation 3.3 can be rewritten as Equation 3.4. This allows the application of the DACM algorithm as a phase unwrapping method in FMCW radar sensing [25].

$$\phi_b[n] = \sum_{k=2}^{n} \frac{I[k](Q[k] - Q[k-1]) - (I[k] - I[k-1])Q[k]}{I[k]^2 + Q[k]^2} \tag{3.4}$$

The second method of phase unwrapping is phase correction. This method works by subtracting 2π from the phase calculated using the arctangent function if $\phi_b[n] - \phi_b[n-1] > \pi$ and adding 2π if $\phi_b[n] - \phi_b[n-1] < -\pi$. It is simpler than the previous method, but is only correct if the real phase only varies less than π between consecutive chirps, or else it is possible that the corrections being made are wrong. Nevertheless, this should not be a problem when acquiring the chest movement signal, as the movement is slow enough to not cause this issue [26]. This method is also used in some of the studies where FMCW is used to measure vital signs [23] [26].

When extracting the chest movement signal, the majority of studies utilize only a single range bin from the range-FFT for each subject. However, in some studies, more than a single range is analyzed, because it is considered that body movements might cause the subject to move between range bins throughout the duration of the data collection or because it is considered that analyzing multiple bins yields better data, even if the subject is not in motion [24] [13]. Some studies also employ a chirp accumulation technique, where for each data point, instead of using data from a single chirp, the range-FFT of multiple successive chirps is added in order to increase the Signal-to-Noise Ratio (SNR) [24] [25]. Lastly, Fang *et al.* [27] did not use phase information in their study, opting to simply use the amplitude of the range bin of each subject over time as the chest movement signal.

3.3.2 Vital Sign Extraction

After the chest movement signal is extracted, the RR and HR can be measured, and once again different studies employ different techniques. Wang *et al.* [25] firstly turn the chest movement signal into

a differential signal, by using the difference between consecutive phase values rather than the phase itself, and then propose two different algorithms to separate the respiration and heartbeat components from this differential signal. In the first of these, the Compressive Sensing based on Orthogonal Matching Pursuit (CS-OMP) algorithm, the signal is first separated into a respiration signal and a heartbeat signal by using two different bandpass filters that leave only the frequency components that correspond to respiration or heartbeat. The CS-OMP algorithm then removes the noise and undesirable harmonics from the signals, leaving only the frequency component that corresponds to respiration or heartbeat. The other method is the Rigrsure Adaptive soft threshold noise reduction based on Discrete Wavelet Transform (RA-DWT) algorithm, in this method the signal is split into two different signals, one for respiration and one for heartbeat, using a wavelet decomposition method. After this, each signal is thresholded in the frequency domain, using an adaptive threshold, to remove noise and finally, the RR and HR are extracted from their respective signals by calculating a reliability metric for the frequency peak in each signal, and if the result is high enough, that is considered to be the RR or HR for that measurement.

One technique that is employed in multiple studies is the Empirical Mode Decomposition (EMD), or a variant of it. EMD decomposes a signal into a number of modes. Each mode is a signal that satisfies the conditions of having the same or nearly the same number of extremes and zero crossings, and the mean value of the upper and lower envelope of the signal being equal to zero. A common variant of this method is the Ensemble Empirical Mode Detection (EEMD), in which multiple iterations of the process are made with random gaussian noise added to the signal in each, after which the mean of each mode is computed and considered to be the result. This leads to a better separation of the signal, usually resulting in more modes being obtained due to less mode mixing, which is the presence of oscillations with very different frequencies in the same mode [30]. Among the FMCW vital sign measuring studies, Fang et al. [27] utilize EEMD to separate the chest movement signal into modes, then identify which of the modes correspond to respiration and heartbeat, and finally determine RR and HR by finding the largest spectral component in their respective modes. Antolinos *et al.* [13] utilize EMD to remove baseline drift from the chest movement signal, after that, the remaining signal is separated into respiration and heartbeat signals using bandpass filters. RR is then measured from the respiration signal and HR and HRV are measured from the heartbeat signal. Sun *et al.* [24] utilize a variation of EEMD, that utilizes adaptive noise instead of random gaussian noise, to separate the heartbeat component of multiple adjacent range bins of the range-FFT. After this, all the detected heartbeat signals from different ranges are analyzed utilizing a Multiple Signal Classification (MUSIC) algorithm and the HR is determined.

Arsalan *et al.* [23], after determining subject range and extracting the I and Q signals for that range,

apply an ellipse fitting algorithm to compensate for smaller errors and then validates the data by calculating the reconstructed circle's deviation from the unit circle, and only accept the data for vital sign measurement if it is under a certain threshold. The phase of the signal over time is then calculated and unwrapped, and an adaptive bandpass filter is used to separate the heartbeat signal from the chest movement signal. The bandwidth of the filter starts out by covering the entire spectrum of possible human HR, however, as new high-quality data is recognized by the algorithm, the band is narrowed down or moved to only include the HR data and filter out unwanted noise and frequency components. HR is calculated by counting the peaks in the heartbeat signal.

Ahmad *et al.* [28], after extracting the chest movement signal and applying phase unwrapping, compute the differential signal of the phase and then use that signal for the rest of the algorithm. Noise is then removed by verifying if there are any outliers within the differential chest movement signal and replacing those with an interpolated value between the previous and next samples. After this, the signal is separated into respiration and heartbeat through the use of bandpass filters, and the heartbeat signal is validated to check if there are any segments with large body movement, and those segments are discarded so that they do not affect the HR measurement. Finally, windowing and gain control are applied to both signals and the vital signs are measured. RR is measured by first computing the FFT of the respiration signal and then verifying what is the largest spectral component and a confidence metric is calculated based on the ratio between the amplitude of the RR frequency component and the rest of the RR frequency range. HR measurement also starts with computing the FFT of the heartbeat signal, but then all the frequency peaks in the HR frequency range are detected and stored, and after some iterations and after removing all peaks corresponding to breathing harmonics, the peak with the most appearances corresponds to the HR value. A confidence metric is also calculated for HR, and if the confidence metrics for RR and HR are too low, a inter-peak distance based method is used instead as a fallback.

Alizadeh *at al.* [26], after phase unwrapping, simply compute the FFT of the chest movement signal and consider the largest spectral components in the RR and HR range to be the RR and HR of the subject. Zhang *et al.* [29] measure RR by discovering the largest spectral component in the FFT of the chest movement signal and then attempt to remove the breathing component and its harmonics through the use of the projection matrix method. After that, HR is determined by detecting the largest spectral component in the remaining signal.

Besides IR-UWB and FMCW radars, continuous wave or Doppler radars have also been used to detect and measure chest movement. This type of radar functions by transmitting a EM wave with continuous frequency and receiving the echo reflected by the OOI. In the majority of literature that utilizes a bioradar

of this type, the chest movement signal is extracted from the phase information of the received signal similarly to an FMCW bioradar. This type of radar is more prone to clutter and interference than an FMCW radar due to not being able to distinguish between different range bins, which makes it bad for use in an environment with a high amount of clutter such as an automotive environment. A study was made using a bioradar of this type in an automotive environment. In this study, Tran *et al.* [31] use a Doppler bioradar with a narrow beam, set up in the steering wheel of the car, to monitor the driver's vital signs, thus avoiding sources of interference by making sure that the driver was the only thing being detected by the radar. However, contrarily to the rest of thee literature that involves this type of radar, chest movement information was extracted from the frequency shift in the echo caused by the Doppler effect, rather than phase information.

Chapter 4

Test Setup

In this chapter, a brief summary of what is expected of each radar is presented, including a comparison between the Ancho and the Onza radar modules, followed by the radar settings and vital sign detection algorithms used for each radar, as well as the procedure for the vehicle tests of the radars. It is divided into multiple sections, one for the radar assessment, one for radar settings and algorithms, which is divided into a subsection for each radar, and one for the test procedure, which was similar for all bioradars.

4.1 Radar Assessment

The different used radar modules have different characteristics, and are therefore expected to perform differently.

The Ancho and Onza radar modules, which are both IR-UWB radar modules, have the advantage of being able to acquire a relatively high amount of frames per second due to needing only to transmit a short pulse and having an ADC that converts the received signal at a high speed. However, their range resolution is much lower in comparison to the RIC60A radar module, due to FMCW radar technology enabling phase analysis, which is not an option in IR-UWB radars. This difference in range resolution could result in a reduced performance when measuring HR, since the motion associated with heartbeat is smaller and thus harder to detect. Finally, because these radar modules are very similar, it would be redundant to test both of them, and their characteristics can be directly compared to one another in order to determine which is the best for this purpose.

Analyzing Tables 1 and 2, it is possible to conclude that the XeThru X4 chip, used by the Onza radar module, has a vastly increased detection range and samples per frame, however, it also has less sampling

rate, which leads to less range resolution, and less PRF in comparison to the XeThru X2 radar chip, used by the Ancho radar module. What this means is that if the use case requires monitoring a larger area, the XeThru X4 chip is better suited due to having much more detection range and samples per frame while keeping a decent range resolution. However, if the area that needs to be monitored is smaller, the XeThru X2 chip is better due to its superior range resolution, despite having a much more limited detection range. PRF also affects radar performance, specifically in terms of framerate, because higher PRF means that each frame is converted from analog to digital faster, and if each frame can be converted faster then more frames can be obtained and processed in the same amount of time, increasing framerate. Considering that the XeThru X2 chip's PRF is more than double of the Xethru X4 chip's PRF, the framerate, in a radar using the X2 chip, will be much higher for the same ADC settings. Taking this into account, and considering that for vital sign detection in an automobile environment the subject is confined to a limited and constant range interval, and that high framerate is desirable, it was decided that the Ancho radar module would be explored and tested and that the Onza radar module would not.

The Xandar Kardian bioradar is harder to evaluate, because the vital sign techniques that it employs are unknown. What is known is that it is also based on an IR-UWB radar module, therefore its advantages and disadvantages should be similar to those of the other two IR-UWB radars, but, without knowledge of how the radar module is being used or how the vital sign detection algorithm functions, any predictions of expected behavior are merely speculative.

Lastly, the RIC60A radar module, due to using FMCW radar technology, has a greater range resolution than the other radars due to the possibility of phase analysis, as was already mentioned in this section. However, because this type of radar requires the transmission of relatively high duration EM waves in the form of chirps, the framerate is much lower in comparison to the IR-UWB radars. On the one hand, the increase in range resolution can be a great advantage when sensing the small chest movements associated with heartbeat, which is beneficial for HR measurements. On the other hand, the decrease in framerate can be harmful and cause a decrease in the measurement performance of both vital signs, because although the regular frequencies of RR and HR are low enough that a very high framerate is not necessary to be able to sample them from the chest movement signal, a lower framerate can still have a negative impact on the quality of the signal.

4.2 Settings and Algorithms

The tested bioradars were all different from each other, therefore each of them had to be configured individually, and different algorithms had to be developed for the bioradars that did not already come with embedded vital sign sensing capabilities. In the following subsections the settings and algorithms used for each bioradar are detailed.

4.2.1 Ancho Bioradar

The settings of this bioradar are mostly related to the XeThru X2 radar chip's ADC, and the center frequency of the transmitted pulse. The settings were optimized in order to maximize the quality of received frames while being able to maintain a framerate of 60 Hz. The specific settings used can be observed in Table 3.

Table 3: Used Acho radar module settings.

ADC minimum	0
ADC maximum	8191
ADC step	8
Pulses per step	16
Iterations	40
Pulse center frequency	7.7 GHz

The used ADC maximum and minimum are the limits of the ADC, and using an ADC step of 8 still leaves 1024 possible values in each iteration, and thus 10 bits of resolution. The high values of pulses per step and iterations assure that the quality of the signal does not degrade due to the conversion process. Trying to reduce the settings to further improve framerate led to a significant decrease in signal quality that would impact the measurements negatively. Furthermore, because the frequency of human heartbeat is lower than 2 Hz, 60 Hz already is significantly above the needed frequency to sample that signal, according to the Nyquist theorem.

The bioradar is intended to measure passenger vital signs in real time, therefore the algorithm should not be too complex and computationally heavy so that the measurements can be done quickly. The applied

techniques are, therefore, relatively simple, but still based on previous research that is described in the state of the art section of this study. A flowchart of the algorithm can be observed in Figure 13.

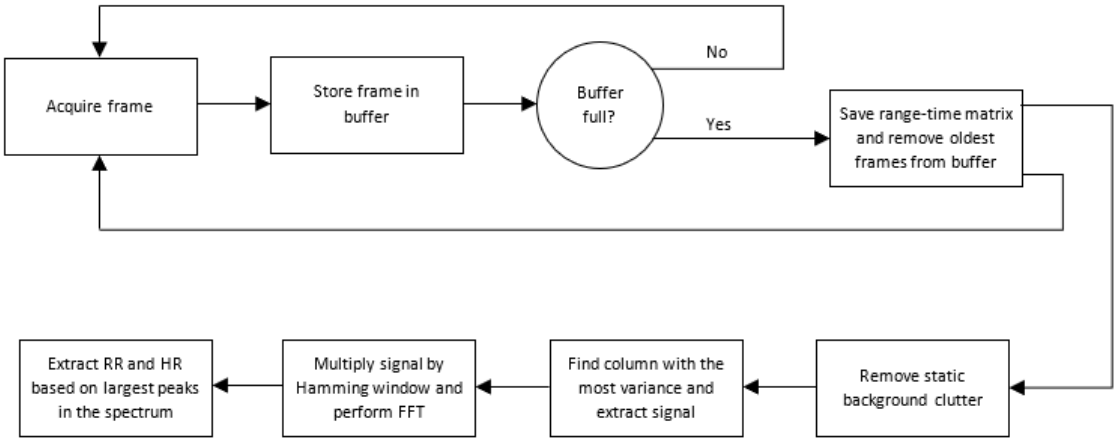

Figure 13: Flowchart of the algorithm for vital sign detection using the Ancho radar module.

In order to acquire radar data, it is necessary to request frames from the radar, these requests are made through a MATLAB command, and the frame is generated by the radar at the time of request. To maintain a steady 60 Hz framerate, a timer is created in MATLAB that requests a frame from the radar at constant intervals, and stores this frame in a buffer, when the buffer is filled, the collected data progresses to the next stage. After this, the older data in the buffer is deleted, and a new timer is created that immediately starts filling the buffer for the next measurement, simultaneously to the signal processing part of the algorithm, so that there is no gap in the data collection. It is important to use a timer so that the framerate is constant, because if that is not the case, then it could lead to errors in later parts of the algorithm when FFTs are computed. However, MATLAB's timer function is not completely reliable, and the framerate is never exactly what is set as the target. Because of that, an estimation of the real framerate is calculated at the end of each data acquisition cycle, and that value is used later when performing the FFT of the chest movement signal.

The size of the buffer must be sufficiently large to be able to measure vital sign data, but not too large as to include data that is too old and therefore irrelevant. After experimentation, it was determined that the correct buffer length was the equivalent to 40 seconds of data. When the buffer is full, the range-time matrix is constructed for the time window, and the data can start to be analyzed. Firstly, static background clutter is removed from the range-time matrix. To do this, one of two methods can be applied as described in the state of the art, namely background subtraction or a loopback filter. Both methods were separately tested as both are computationally simple. An example of the results of static background removal can be

seen in Figure 14, using background subtraction. In Figure 14a, many columns of the range-time matrix exhibit detections that are caused by static background clutter, however, in Figure 14b, after background subtraction is applied, the vast majority of clutter is gone and the subject range can be easily distinguished.

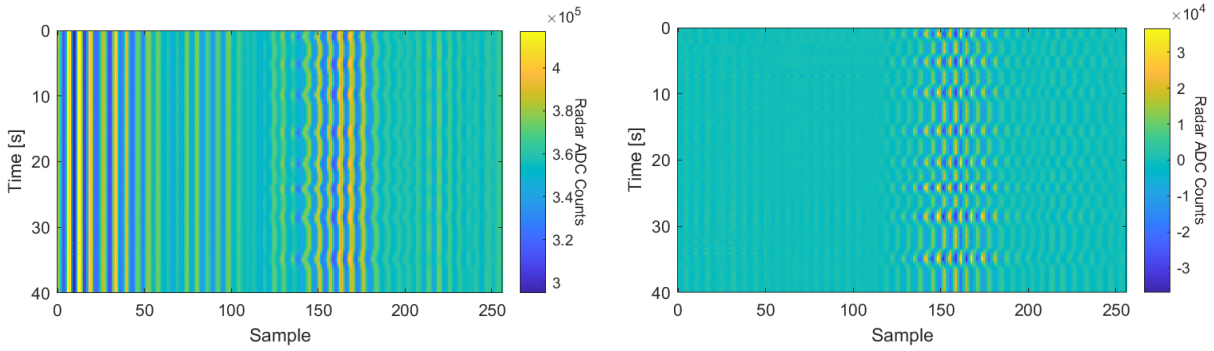

Figure 14: Example of range-time matrix from Ancho radar module data: a) Before static background clutter removal; b) After static background clutter removal.

After this, subject range is determined through finding which column of the range-time matrix has the most variance, and the chest movement signal is extracted from that column, an example of the chest movement signal for a single 40-second window of time can be observed in Figure 15a. In this example the respiration component of the chest movement signal can be easily observed, along with the heartbeat component and some noise. The signal is then multiplied by a Hamming window before its FFT is computed. Multiplying the signal by a Hamming window reduces the presence of spectral leakage in the signal's FFT [32], which could affect the next stage of the algorithm. After windowing, the FFT of the signal is computed. Finally, the largest peaks of the spectrum within the frequency intervals corresponding to RR and HR are found, and the frequency they correspond to is considered to be the RR and HR of the subject. An example of this can be seen in Figure 15b. In this figure, the peaks for both RR and HR are highlighted, respectively, in green and red, as well as the frequency intervals that correspond to each vital sign. The frequency interval for RR is from 0.13 Hz to 0.43 Hz, and the frequency interval for HR is from 0.83 Hz to 2 Hz. After detection, the measurements are converted to breaths per minute or beats per minute by multiplying the value in Hertz by 60. These measurements are not the instantaneous values of RR and HR, but rather the average value of these vital signs for the time corresponding to the data that was used. For measurements beyond the first, a weighted average is used between the previous and current measurements, this technique prevents anomalous results from affecting the measurements too much, while still being able to track slow, natural changes in the measureed vital signs.

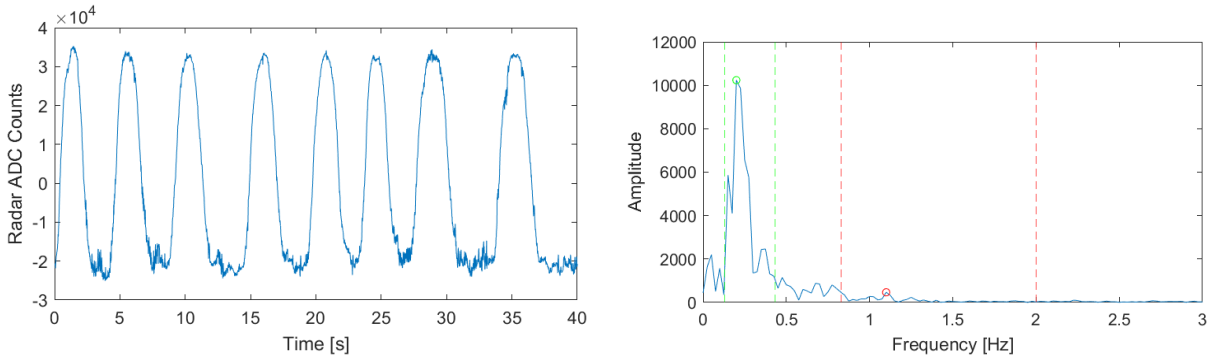

(a) (b)

Figure 15: Examples of: a) a chest movement signal obtained using the Ancho radar module b) the FFT of that signal, with the detection limits and detected vital sign peaks for RR and HR.

After RR and HR measurements are made, the algorithm waits until the buffer is full again before making another measurement with the new data. It should be noted that the buffer is not completely cleared between each data collection cycle, only the oldest frames in the buffer are removed. Using this sliding window technique, each measurement utilizes 40 seconds of data but measurements can be made more often than every 40 seconds, and consecutive measurements share the majority of their data. In addition to this, although the described algorithm is for performing live measurements, the results of this study were obtained using prerecorded raw data, so that different processing techniques could be applied to the same dataset to make direct comparisons. Because of this, the time between measurements can also be as low as desired, as there is no pressure to perform each measurement before the end of the next data collection cycle.

4.2.2 Xandar Kardian Bioradar

There is very little configuration in this bioradar, and, as previously mentioned, the algorithm that it uses is unknown. The only setting that can be changed using the app provided by the manufacturer is the maximum detection range of the device, which was set to 1.11 meters, which is the minimum value for this setting, but enough to detect the subject in the tests. Having this value be low as possible also reduces the amount of background noise that can possibly interfere with the measurements.

Even though the algorithm is unknown, it can be observed that since the RR and HR measurements start as soon as human presence is detected, the algorithm is able to output instantaneous vital sign measurements, unlike the algorithm that was developed for the Ancho radar module, which only outputs average values of the vital signs for each period of time. As for the reliability metric, it is clearly tied to

the amount of detected movement, as it only increases after the subject stands still for a few seconds, and if the subject moves too much it quickly drops back to zero. However, even if the subject is standing completely still, in some cases the reliability does not increase to high values, so therefore there must be more factors that are taken into account when calculating reliability. Nonetheless, these assumptions are merely based on how the bioradar appears to operate, and it is not possible to be completely sure that they are correct.

4.2.3 RIC60A Bioradar

The settings for this radar are more complex and in-depth than the rest of the radars used in this study. As previously mentioned, this radar's settings are selected using a program supplied by the manufacturer. The used settings can be observed in Figure 16. These are based on the settings recommended by the manufacturer for FMCW radar, but with one of the receiving antennas disabled, as it was not necessary for this purpose.

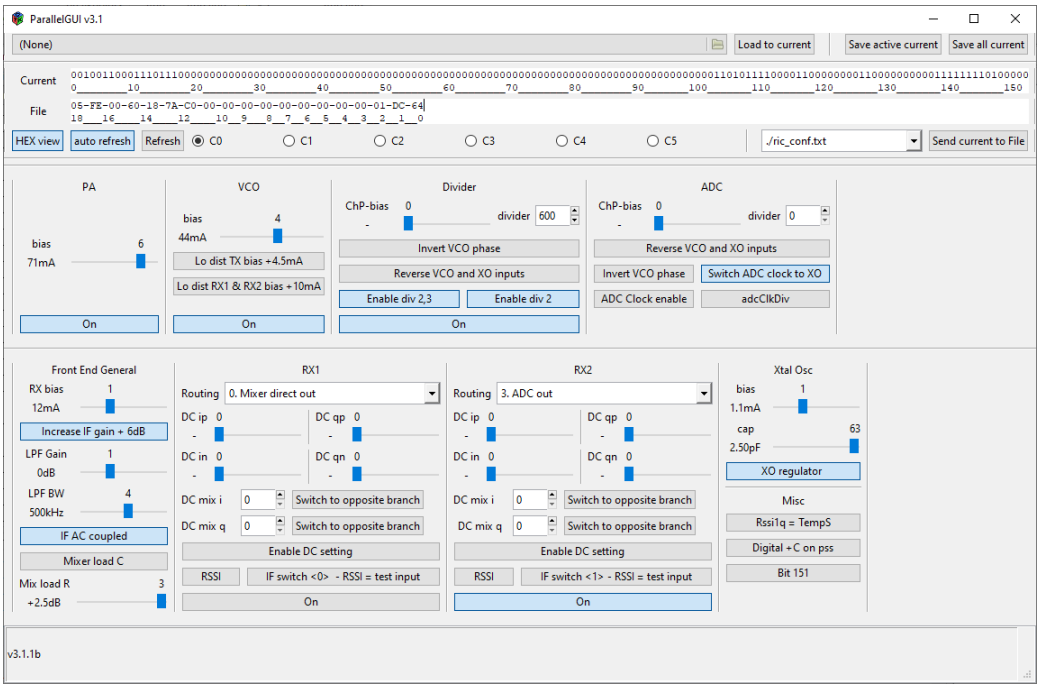

Figure 16: Settings used with the RIC60A radar module.

Besides these settings, the chirp shape and duration must also be defined before measurements can be made. Chirps are requested using a MATLAB command, and multiple chirps can be requested at the same time, in which case they are performed immediately one after the other. For this study, the chosen chirp shape was sawtooth, and three chirps were requested at a time. Because chirps are done

in succession and the full bandwidth of the transmitter was used, it is not realistic to instantly change the VCO voltage from maximum to minimum between each chirp as the hardware cannot follow that rate of change, so a small 1 ms long recovery period is added to the end of each chirp. As such, an example of the transmitted frequency over time of three consecutive 10 ms long chirps can be observed in Figure 17. The full bandwidth of the radar is also used.

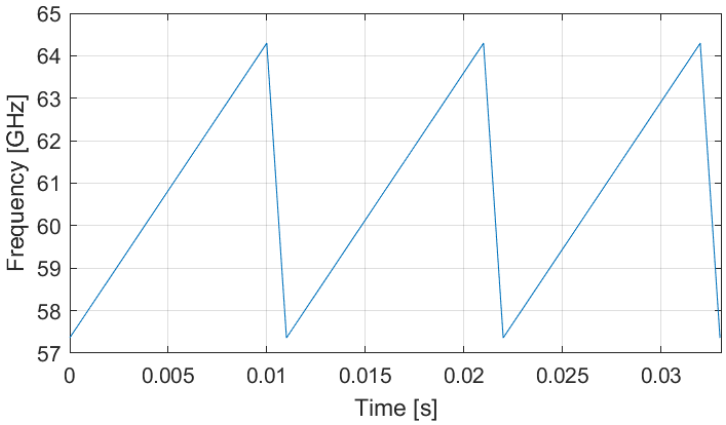

Figure 17: Example of three triangular chirps in succession with a recovery period at the end of each.

Two different configurations for chirp time and frames per second were tested, one with longer chirp time and a lower framerate, and another with longer chirp time but higher framerate. A longer chirp time increases the quality of the signal, but a higher framerate can also be advantageous to better detect the chest movement, especially the heartbeat component. The differences between the two configurations can be observed in Table 4.

Table 4: Differences in chirp settings between the two RIC60A radar module sets.

	Set 1	Set 2
Chirp time	15 ms	10 ms
Frames per second	8	12

The vital sign measurement algorithm used in this bioradar is also based on obtaining the FFT of the subject's chest movement signal, however, because FMCW radar is very different from IR-UWB radar, the techniques that are used are different. A flowchart of the algorithm for live vital sign detection using the RIC60A radar module can be seen in Figure 18.

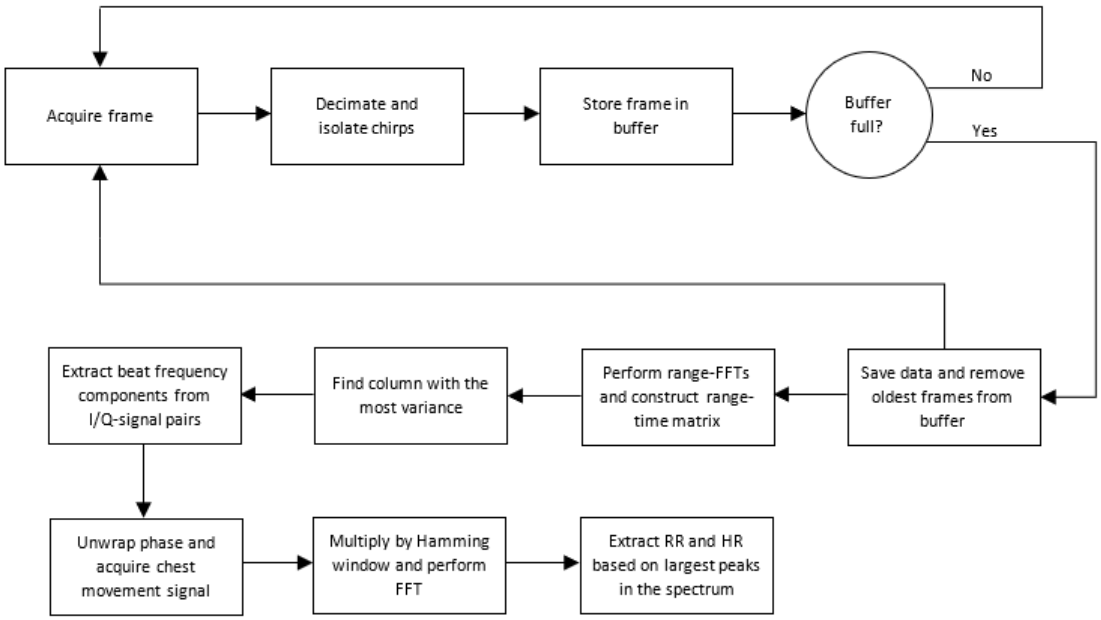

Figure 18: Flowchart of the algorithm for vital sign detection using the RIC60A radar module.

The data acquisition section of the algorithm is similar to the data acquisition section of the previous bioradar, with MATLAB timers ensuring that it is made with a stable framerate and the chirps being stored in a buffer until enough data has been collected. However, two problems need to be addressed that were not present in the other bioradar, specifically the large size of the data due to the high sampling rate of the ADC, and the existence of parts of the IF signal that are not valid data due to the chirp recovery time. The radar's ADC has a sampling rate of 25 MHz, which allows it to sample high frequency components of the IF signal. However, this amount of sampling rate is not necessary for this use case, because the chirp times are long enough that the frequency varies slowly and the target is close to the radar. Using as an example Equation 2.8, with a chirp time of 10 ms and the full bandwidth of the radar, a target standing 2 meters away from the radar would have a beat frequency of less than 1 KHz, which could easily be sampled with a fraction of the ADC's sample rate. Taking this into account, considering that the sample rate of the radar module's internal ADC cannot be changed and such a large amount of samples puts unnecessary computational strain on the system, a MATLAB function was used to decimate the signal down to a lower sampling rate. This function also applies a lowpass filter to the signal prior to decimation, which is necessary when performing this operation. A decimation factor of 1000 was used, effectively reducing the sampling rate of the IF signal to 25 KHz, which is still more than what is necessary for the intended use.

After this, the invalid parts of the signal must still be removed. The IF signal has the same duration as the sweep, including the recovery time at the end of each chirp, however, the sections that correspond to

the recovery time are not usable data, as the rate of frequency variation is different from the chirp and is also not constant, because this part of the chirp is not calibrated in accordance to the VCO frequency curve. Because of this, these parts of the IF signal are removed. The first chirp of each frame is also discarded, as recommended by the manufacturer, because it normally has a high amount of noise. Finally, the frame is stored in the buffer and the process repeats until the buffer is full. When that happens, like with the Ancho radar module, the data is saved and the processing begins, while new data is collected simultaneously for the next measurement.

When analyzing the data, from each frame, the I-signal and Q-signal are separated, then, each of these signals is multiplied by a Hamming window function to avoid spectral leakage, and their range-FFTs are computed. A range-time matrix is made for each of these signals using their respective range-FFTs from all the frames in the data. After this, the column of the I-signal range-time matrix with the most variance in its absolute values is considered to correspond to the subject range, and to the beat frequency of the subject. The columns corresponding to the closest ranges to the radar are ignored at this stage, as it is possible that those have major interference that could result in false positives. An example of this operation can be observed in Figure 19. As can be seen in the graph, the highest peak is situated at about 3000 Hz, which would be the beat frequency that corresponds to the subject range.

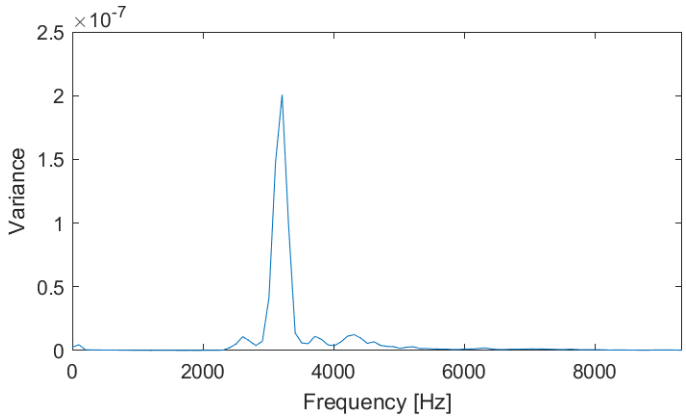

Figure 19: Example of subject range estimation in the RIC60 radar module vital sign detection algorithm.

After the subject range is determined, the phase signal for that range must be extracted. For this stage of the algorithm, two different phase unwrapping methods were tested to deal with the problem of phase ambiguity. The used methods were phase correction and the DACM algorithm, as described in the state of the art chapter. In both cases, the columns of the I-signal and Q-signal range-time matrices that correspond to the subject range are extracted, creating a pair of I-signal and Q-signal beat frequency amplitude and phase over time, with each value having a real component corresponding to amplitude and an imaginary value corresponding to phase. In theory, the I-signal beat frequency components should

only have a real component, and the Q-signal beat frequency components only an imaginary component. However, this is not the case when looking at the data at this point in the algorithm due to limitations in the hardware. To solve this problem, only the real part of the I-signal frequency components and the imaginary part of the Q-signal frequency components are used when applying the phase unwrapping algorithms. In the case of phase correction, a MATLAB function is used to calculate the phase before correction using the signals as described above. In the case of the DACM algorithm, the signals are used as the $I[n]$ and $Q[n]$ signals in Equation 3.4. An example of phase unwrapping can be seen in Figure 20. In Figure 20a, the chest movement signal shows severe phase wrapping by being limited to the interval between $-\pi$ and π, which causes large discontinuities in multiple places along the signal, however, in Figure 20b, after the phase correction method has been applied, the discontinuities are gone and the chest movement signal is recognizable, with the larger oscillations that correspond to the respiration component and smaller oscillations that correspond to the heartbeat component, as well as clutter. Once phase unwrapping has been performed, the chest movement signal is ready for vital sign measurements.

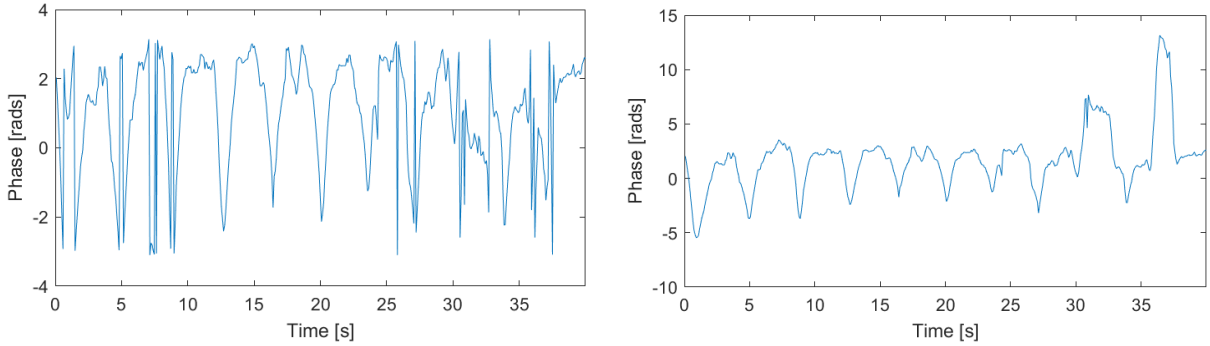

(a) (b)

Figure 20: Example of the chest movement signal acquired using the RIC60A radar module: a) Before phase unwrapping; b) After phase unwrapping.

Using the chest movement signal, the RR and HR measurements are performed in the same way as the measurements with the Ancho radar module. The FFT of the chest movement signal is computed after multiplication by a Hamming window, and the largest peaks in frequency components inside the intervals for RR and HR are considered to be the RR or HR for the time period of the analyzed data. The weighted average between the previous and current measurements used in the Ancho radar module algorithm is also applied here, for the same reasons. The buffer size for each measurement is 40 seconds, and in order to make frequent measurements the sliding window technique is used. Two options for used data were explored, one where only the data from the third chirp was used, and another where the differential between I/Q-signal pair of the second and third chirp was used. This was done to test if the differential could provide an advantage in filtering out static background clutter.

4.3 Test Procedure

The test procedure was as uniform as possible between all the tested bioradars. Every bioradar was tested in the same vehicle, a Mercedes Class V van, modified so that the back seats were facing each other and with an added frame for device setup. The subject was seated in one of the back seats, and the radar was placed in front of the subject, aiming at their chest. Because each radar module had a different way of being affixed to the vehicle's internal structure, the distance to the subject varies between each bioradar. In Figure 21, the used setup can be observed, with the white square representing the approximate position of the bioradar, and the green circle being the subject.

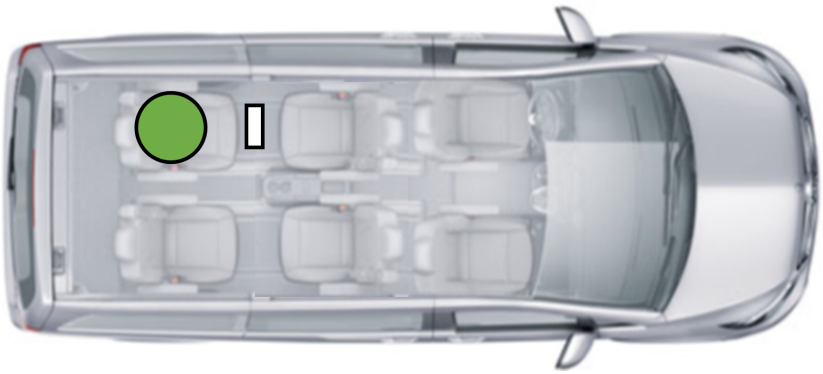

Figure 21: Setup of radar and subject inside the vehicle.

Raw data recordings were made using the Ancho radar module and the RIC60A radar module, so that the data could be better analyzed later and so that different algorithms could be compared using the same dataset. As for the Xandar Kardian bioradar, periods of vital sign measurements were made and saved for later analysis. While data recordings or vital sign measurements were being made, the subject's vital signs were measured using a Zephyr BioHarness, and the vital sign measurements made by this device were also saved to be used as ground truth. Data recordings were made with the vehicle stationary and in motion through an urban area.

A total of six raw data recordings were made using the Ancho radar module, three with the vehicle stationary and three with the vehicle in motion. Each recording has a duration of two minutes and a framerate of 60 frames per second. The recordings were made using a MATLAB script that followed the data acquisition process described in the previous section, without performing any data processing or vital sign measurements. The data from each recording data was saved in a *.mat* file, that included the raw data, the used radar settings, the framerate of the recording and a timestamp.

To test the Xandar Kardian bioradar, two vital sign measurement recordings were made, one when the

vehicle was stationary and another when the vehicle was in motion. Before the tests, the radar was setup in accordance to the manufacturer's recommendations, and was calibrated using the automatic calibration process with no one inside the vehicle. Each recording had a duration of five minutes and the data of each recording was automatically saved by the bioradar's app in a *.txt* file where each line corresponds to a single measurement pair, with all the data sent by the radar module to the computer, including not only the RR and HR measurements, but also a timestamp, the reliability of these measurements and the movement reliability among other data.

Using the bioradar based on the RIC60A radar module, eight raw data recordings were made in total, four for each set in Table 4, with two being when the vehicle was stationary and the other two with the vehicle in motion. Each recording had a duration of two minutes and was made using a MATLAB script that recorded the data in accordance to the data collection part of this bioradar's algorithm, including the decimation of the I/Q signal and removal of unwanted parts. The data from each recording was stored, similarly to the data from the first bioradar, in a *.mat* file containing the raw data, radar settings and important characteristics of the recording, such as true framerate, sampling rate of the I/Q signal pair after decimation, and a timestamp.

The Zephyr BioHarness vital sign measurements are stored in a *.txt* file that is accompanied by another file that includes the timestamp for the start of data acquisition. The main file contains the RR and HR measurements, but, instead of the exact time of each measurement, contains only the elapsed time since the start of data acquisition. Because of this, the supporting file is necessary to be able to locate the vital sign measurements in time and therefore be able to compare them with the measurements from each bioradar.

In data analysis, for each of the raw data recordings, the data was processed in accordance to the algorithm of the corresponding bioradar, with the same data being used to test multiple variations of the same algorithm. For both the Ancho radar module and RIC60A radar module, the first RR and HR measurements were made using the first 40 seconds of recorded data, with a measurement being made for each second from there on out, using the previous 40 seconds of data. For the Xandar Kardian bioradar vital sign measurements, even though each measurement had a timestamp, the timestamps' resolution was only up to the second, with multiple measurements being made each second, and therefore having the same timestamp. Because of this, an average of the measurements was calculated for each second, and that average was considered to be the measured RR, HR, RR reliability or HR reliability for that second. To be able to compare the RR and HR measurements made by the bioradars with the ground truth obtained using the Zephyr BioHarness, the ground truth measurements had to be converted to match the way the

radar measurements are made, because while each bioradar measurement takes into account a larger period of time, the ground truth measurements are instantaneous values for RR and HR. To do this, for each radar measurement, a ground truth datapoint was made using the average of RR and HR ground truth measurements from the period of time that was considered in the bioradar measurement. For example, the ground truth equivalent for a RR measurement made by the Ancho radar module bioradar is the average of the RR measurements made by the Zephyr BioHarness in the 40 seconds before the point in time where the bioradar's RR measurement is located.

After a ground truth measurement was generated for each radar measurement, the performance of each bioradar and algorithm was evaluated by calculating the Mean Relative Error (MRE) for each set of RR or HR measurements using the formula in Equation 4.1, where v_m is a set of RR or HR measurements, v_t is the corresponding set of ground truth measurements and n is the total number of measurements in v_t.

$$MRE = \frac{\sum_{k=1}^{n} || \frac{v_m(k) - v_t(k)}{v_t(k)} ||}{n} \cdot 100\% \tag{4.1}$$

Chapter 5

Results and Discussion

In this chapter, the results of each of the bioradars and their different algorithms are displayed and discussed. It is divided in four sections, one for each bioradar, which are further divided into subsections for results and discussion, and a final section with a comparison of the best results from each bioradar.

5.1 Ancho Bioradar

The results for this bioradar are based on a total of six raw data recordings made in an automotive environment, three when the vehicle was stopped and another three when the vehicle was in motion, each with a duration of two minutes.

5.1.1 Results

Two variations of the algorithm for this bioradar were tested using the raw data recordings. The difference between the variations is in the static background clutter removal step, where one used the background subtraction method and the other used the loopback filter. For the loopback filter, it was determined that the best value of the weighting constant is $\alpha = 0.93$, because this provided the best results for the collected raw data. An example of an obtained chest movement signal by applying each algorithm to the same data from one of the stationary vehicle recordings can be seen in Figure 22, with Figure 22a being the result of background subtraction and 22b the result of using a loopback filter.

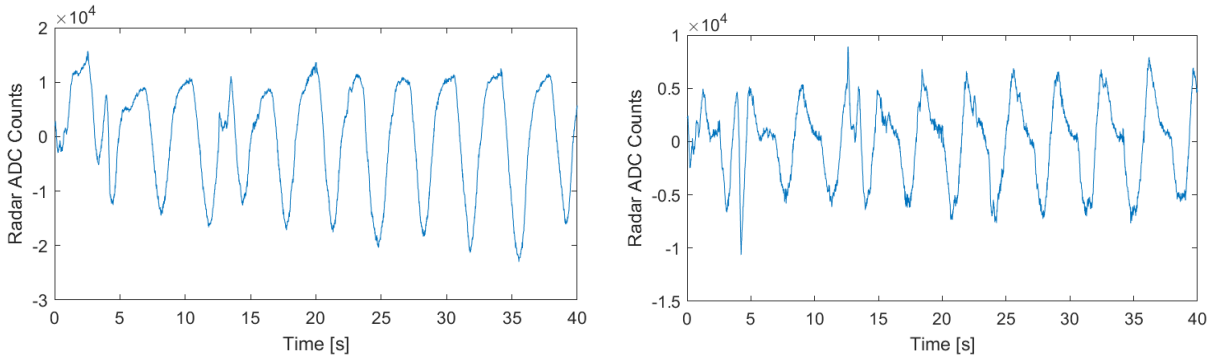

(a) (b)

Figure 22: Example of chest movement signal obtained after applying different methods of static background clutter removal methods: a) Background subtraction; b) Loopback filter.

The FFTs of the chest movement signals present in Figure 22 can be observed in Figure 23, where Figure 23a is the FFT of the signal in Figure 22a, in which background subtraction was used, and Figure 23b is the FFT of the signal in Figure 22b, in which the loopback filter was used. In these figures, the green dashed lines represent the limits of the RR peak detection interval, the red dashed lines represent the limits of HR peak detection interval, the green circle represents the RR peak and the red circle represents the HR peak.

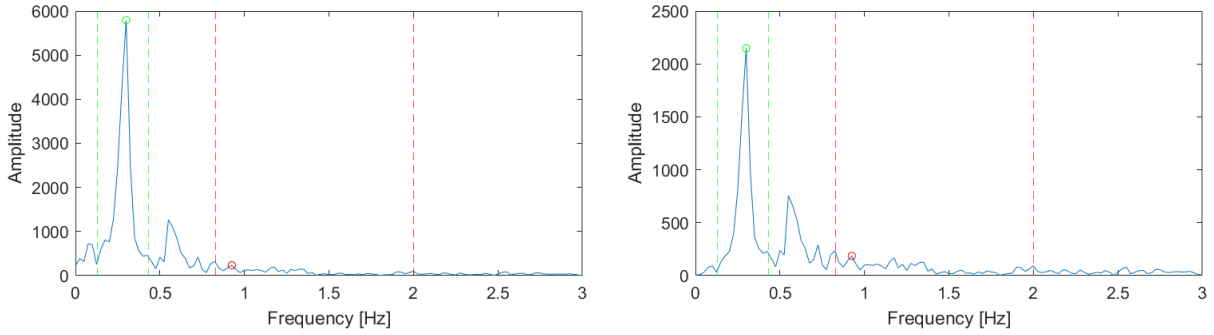

(a) (b)

Figure 23: Example of the FFTs of the chest movement signal obtained after applying different methods of static background clutter removal methods: a) Background subtraction; b) Loopback filter.

An example of the measured vital signs versus ground truth for the third stationary vehicle recording with the different methods can also be seen in Figure 24. In Figures 24a and 24b, HR measurements obtained using, respectively, background subtraction and loopback filter, can be seen.

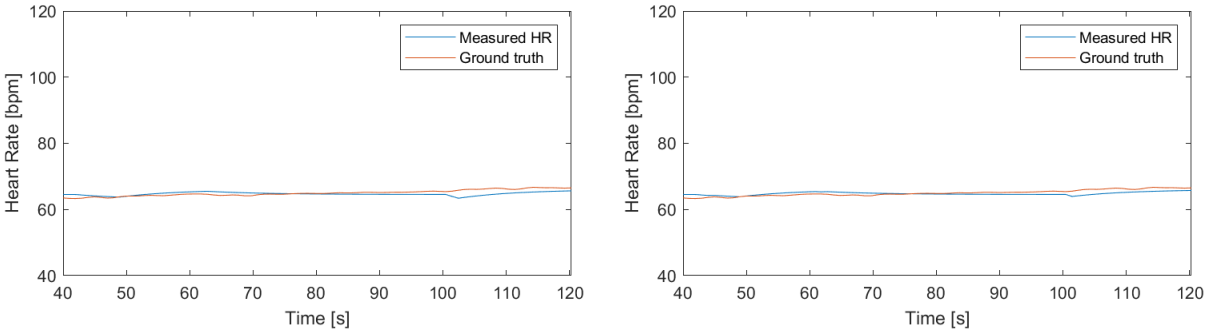

Figure 24: Examples of measured HR using the different static background clutter removal algorithms, in comparison to ground truth: a) HR measurements using background subtraction; b) HR measurements using loopback filter.

The detailed results, with the MRE for each raw data recording and static background clutter removal technique, can be seen in Tables 5 and 6, Table 5 corresponding to the results using the background subtraction, and Table 6 corresponding to the results using the loopback filter. The average MRE for each vital sign in each situation can also be seen in both tables.

Table 5: Ancho radar module performance using the background subtraction method for static background clutter removal.

	Stationary vehicle recordings				Moving vehicle recordings			
	Rec. 1	Rec. 2	Rec. 3	Average	Rec. 1	Rec. 2	Rec. 3	Average
RR MRE (%)	7.66	5.53	8.35	7.18	14.01	3.84	12.73	10.19
HR MRE (%)	3.62	8.75	1.22	4.53	9.72	12.96	12.35	11.68

Table 6: Ancho radar module performance using the loopback filter method for static background clutter removal.

	Stationary vehicle recordings				Moving vehicle recordings			
	Rec. 1	Rec. 2	Rec. 3	Average	Rec. 1	Rec. 2	Rec. 3	Average
RR MRE (%)	7.01	3.50	8.33	6.28	9.75	4.25	12.48	8.83
HR MRE (%)	3.60	7.18	1.10	3.96	9.95	10.87	9.12	9.98

5.1.2 Discussion

In the analysis of this bioradar's results, the main focus is on comparing the performance of the two versions of the algorithm in order to determine which method of static background clutter is better for this purpose.

When comparing the chest movement signals in Figure 22, some differences between the two methods can be seen. In Figure 22a, which corresponds to a chest movement signal obtained with the version of the algorithm that uses the background subtraction method, the respiratory component of the signal is clearly visible in the periodic high amplitude fluctuations. However, the heartbeat component is not so clearly present. Even though smaller variations can also be seen, it is unclear whether they correspond to the heartbeat or simply noise. In comparison, the chest movement signal obtained with the the version of the algorithm that uses the loopback filter method, visible in Figure 22b, has a less clear respiratory component as the corresponding oscillation is distorted by the filtering. On the other hand, the heartbeat component is clearer, as smaller oscillations and peaks can be seen amid the signal. This difference between the signals is due to the loopback filter, as it acts like a highpass filter, suppressing the respiratory component due to its lower frequency but leaving the heartbeat component intact, which amplifies it in relation to the respiratory component. This becomes apparent when looking at the FFTs of these signals in Figure 23, where in Figure 23a, the FFT of the signal in Figure 22a, the frequency of the RR peak is the same as in Figure 23b, the FFT of the signal in Figure 22b, but with decreased amplitude. Furthermore, higher frequency components are less suppressed and the HR frequency interval is not suppressed at all, and the FFTs are similar except for this filtering. It can also be said that in both of these figures, the detected HR peak is unlikely to correspond to the subject's real HR, as it corresponds to the third harmonic of the RR frequency peak.

Another aspect of the algorithm is the weighted average made between the previous measurement and the current in order to avoid large erroneous changes between successive measurements, this is useful when the measurements are mostly correct, as can be seen in Figures 24a and 24b, where, in both of them, there is small spike downwards shortly after 100 seconds which is caused by a wrong measurement and would have introduced greater error if not for this averaging method. On the other hand, if the vital sign measurement is wrong, it will take more cycles of correct measurements to compensate, which can also be seen in the final HR measurements in Figures 24a and 24b. Due to this, perhaps an outlier detection and removal method would be more appropriate and effective in improving results.

When comparing the results of the two versions of the algorithm, by analyzing Tables 5 and 6, it is

clear that the version of the algorithm with the loopback filter has better performance than the background subtraction version. The loopback filter version has lower average MRE in both situations for both RR and HR, it has better performance in all recordings for both vital signs when the vehicle is stationary, and only has slightly worse performance when measuring HR on the first moving vehicle recording and when measuring RR on the second vehicle recording. This is because the loopback filter method is capable of nullifying slow changes in the environment over time, contrarily to the background subtraction method, which cannot adapt to changes at all. In an automotive environment, which can be very dynamic, being able to adapt to changes in the environment is important and thus these results are expected. The performance when the vehicle is in motion is worse than when the vehicle is stationary. This is due to there being more sources of interference when the vehicle is in motion as well as to sources of interference that already existed when the vehicle was stationary being amplified. When the vehicle is stationary, the main sources of interference are the inside of the vehicle itself, which has many metallic components that cause clutter, and the body movements of the subject. When the vehicle is in motion, there are also the vibrations caused by the vehicle's engine and the road, and the subject has more body movement that is very difficult to avoid due to the movement of the car when turning, accelerating and braking. Because of this, the decrease in performance between the stationary vehicle recordings and the moving vehicle recordings is expected. This difference is more notable when measuring HR, which is also expected because, as the heartbeat component is much smaller than the respiratory component in the chest movement signal, it is more affected by the presence of noise than the respiratory component.

5.2 Xandar Kardian Bioradar

For this radar, instead of raw data recordings, two vital sign measurement periods were recorded, one with the vehicle stationary and another with the vehicle in motion, each with a duration of five minutes. As there are no alternative algorithms to be compared, the performance of the bioradar is simply measured by comparing the acquired measurements to the ground truth. However, it should be noted that a reliability metric is associated with each measurement, and measurements that have low reliability should be less relevant as the bioradar itself acknowledges that these are not reliable.

5.2.1 Results

With the reliability score in mind, Figure 25 shows how the vital sign measurements compare to ground truth when the vehicle is stationary, with Figure 25a showing the RR measurements and Figure 25b showing the HR measurements. Figure 26 shows the reliability over time for both vital signs when the vehicle is stationary, with Figure 26a showing the reliability of the RR measurements and Figure 26b showing the reliability of the HR measurements. As for the moving vehicle test, in Figure 27 it can be seen how the vital sign measurements compare to the ground truth when the vehicle is in motion, with Figure 27a showing the performance of RR measurements and Figure 27b showing the performance of HR measurements. Figure 28 shows the reliability of the vital sign measurements when the vehcile is in motion, with Figure 28a showing the reliability of the RR measurements and Figure 28b showing the reliability of the HR measurements.

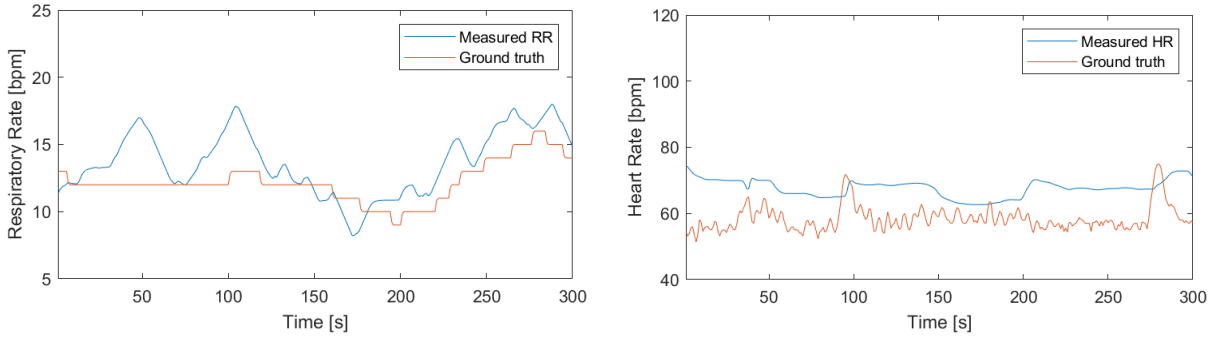

(a) (b)

Figure 25: Vital sign measurements made by the Xandar Kardian bioradar when the vehicle is stationary, in comparison to ground truth: a) RR measurements; b) HR measurements.

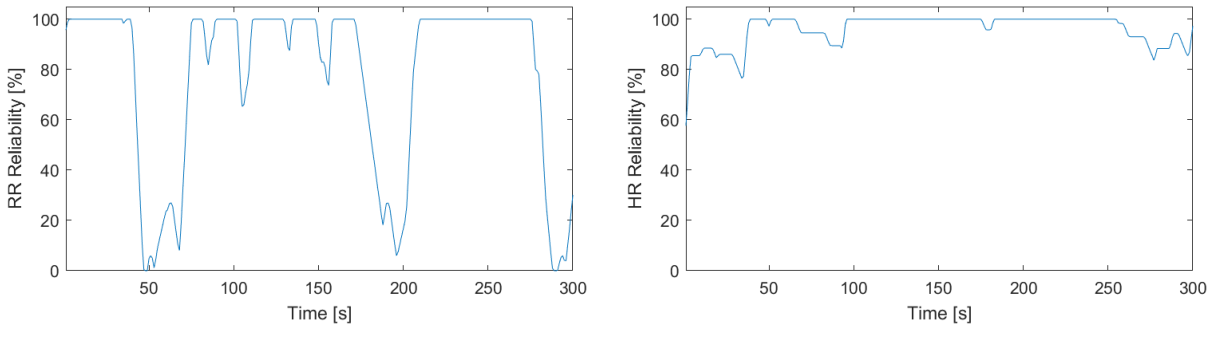

(a) (b)

Figure 26: Reliability of the vital measurements made by the Xandar Kardian bioradar when the vehicle is stationary: a) Reliability of RR measurements; b) Reliability of HR measurements.

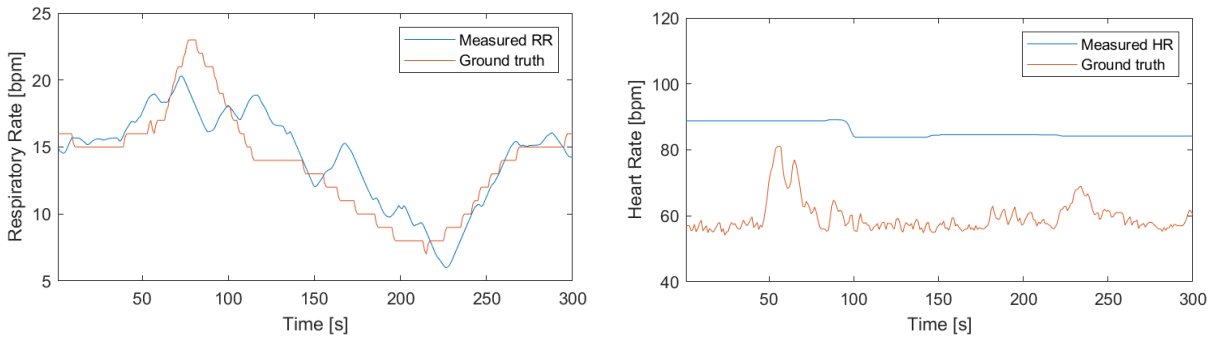

(a) (b)

Figure 27: Vital sign measurements made by the Xandar Kardian bioradar when the vehicle is moving, in comparison to ground truth: a) RR measurements; b) HR measurements.

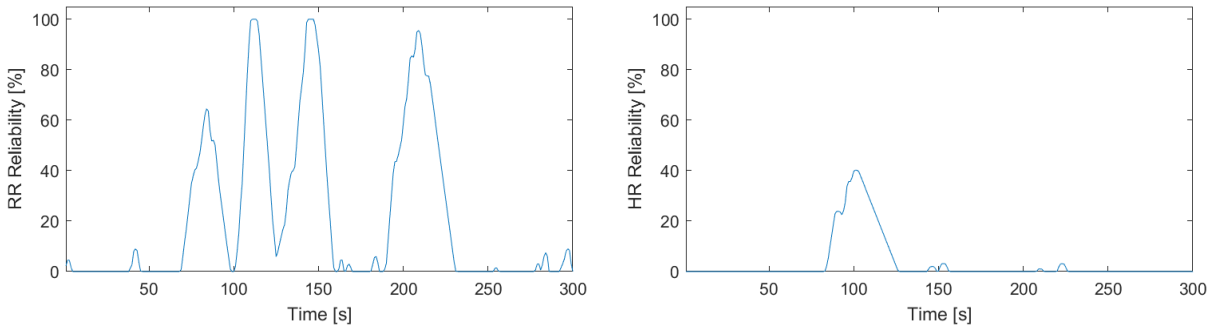

(a) (b)

Figure 28: Reliability of the vital measurements made by the Xandar Kardian bioradar when the vehicle is moving: a) Reliability of RR measurements; b) Reliability of HR measurements.

The detailed results can be seen in Table 7, which includes the MRE for each vital sign and vehicle situation, the average reliability for each of these and, in order to account for reliability, and adjusted MRE statistic that only takes into account the relative error of measurements with a reliability over 85 % when calculating MRE. This is done so that the measurements that are considered unreliable by the sensor itself are discarded. There is no adjusted MRE statistic for the moving vehicle HR measurements because, as can be seen in Figure 28b, the reliability was never over 85 % throughout the entire test.

Table 7: Xandar Kardian bioradar performance.

	Stationary vehicle		Moving vehicle	
	RR	HR	RR	HR
MRE (%)	14.38	16.83	12.00	44.73
Average reliability (%)	77.27	95.97	22.06	3.33
Adjusted MRE (%)	13.36	15.60	14.11	-

5.2.2 Discussion

There is no comparison to be made between the performance of different algorithms when evaluating this bioradar, and the exact algorithm that it uses is not known. However, the results that were obtained can still be analyzed and later compared to the results of the other bioradars.

Looking at Figure 25a, it can be seen that while the measurements are relatively good at following the real values of RR when the vehicle is stationary, there are some sudden spikes in the measurement that are not found in the ground truth, the largest of these being at around 50 and 100 seconds of the test. These spikes, however, coincide with decreases in reliability, as can be seen in Figure 26a, so the bioradar itself is aware that the quality of measurements had a decrease in that time period. On the other hand, there are other deviations from the ground truth that do not have corresponding decreases in reliability, and decreases in reliability that do not correspond to erroneous measurements, therefore the reliability score determined by the bioradar is not a precise indicator of the quality of measurements. This becomes more apparent in the HR measurements and reliability in Figures 25b and 26b, where even though the reliability stays relatively high for most of the test, the HR measurements are not very close to the ground truth. Nevertheless, the reliability metric should be considered when evaluating the bioradar's performance.

When the vehicle is in motion, RR measurements appear to be as good as when it is stationary, as can be seen in Figure 27a, even though reliability is much lower in general, as can be seen in Figure 28a, only reaching high values for short periods of time. When the vehicle is in motion the HR measurements are much worse than when it is stationary. As can be seen in Figure 27b, it does not appear to be correlated with the ground truth at all, and, as can be seen in Figure 28b, reliability stays a 0 % for most of the time, only increasing for a short period to a value still less than 50 %, and going back to 0 % shortly after. This means that this bioradar struggles to perform HR measurements when the vehicle is in motion, and recognizes it, as is evidenced by the very low values of reliability.

These results are confirmed when looking at the data in Table 7. The MRE for RR measurements actually decreases slightly when the vehicle is in motion instead of increasing as expected, suggesting that this bioradar is not affected by the increased noise and interference when measuring RR, even though the average reliability decreases compared to when the vehicle is stationary. As for HR, the MRE increases significantly when comparing the performance from the stationary vehicle test with the performance from the moving vehicle test, to the point where the measurements are essentially completely wrong. In addition to this, the average reliability is also extremely low, at less than 5 %, and was never higher than 85 %. When looking at the MRE adjusted to reliability, we can see that when the vehicle is stationary both RR

and HR measurements are better when only considering measurements with more than 85 % reliability, even though the improvement is very small. When looking at the same statistic on the moving vehicle test, we can see that only considering the measurements with more than 85 % reliability actually decreases the average MRE of RR measurements, which is unexpected since considering only high reliability measurements should be better than considering all measurements. On the other hand, this statistic is not available for the HR measurements because the reliability was always lower than 85 % for that vital sign throughout the entire moving vehicle test. Overall, this might mean that even though the RR measurement quality is consistent between the stationary and moving vehicle tests, the reliability calculation is not accurate when the vehicle is in motion, as ignoring low reliability measurement worsens the bioradar's performance when measuring RR. HR measurement quality is very poor when the vehicle is in motion, to the point where the HR measurements are not reliable at all, but reliability is also very low, so the bioradar itself is aware of the inability to perform HR measurements in those conditions.

5.3 RIC60A Bioradar

The results of this bioradar are based on a total of eight raw data recordings made in an automotive environment. These recordings have a duration of two minutes each and are split in two sets with four raw data recordings each, obtained with different radar settings, which are described in Table 4, and within each set two recordings were made with the vehicle stopped and the other two with the vehicle in motion.

5.3.1 Results

A total of four combinations of algorithms were tested, as there are two methods for which data to use, single chirp and differential, and two methods for phase unwrapping, phase correction and the DACM algorithm. Furthermore, the dataset is also split into two parts, that were obtained using different settings, as described in Table 4. An example of a chest movement signal extracted from the same raw data of a stationary vehicle recording using different combinations of techniques can be seen in Figure 29. The signals obtained using single chirp data are represented in Figures 29a and 29b, with phase unwrapping performed using the DACM algorithm and the phase correction method, respectively. The signals obtained using differential data are represented in Figures 29c and 29d, with phase unwrapping performed, once

again, using the DACM algorithm and the phase correction method, respectively.

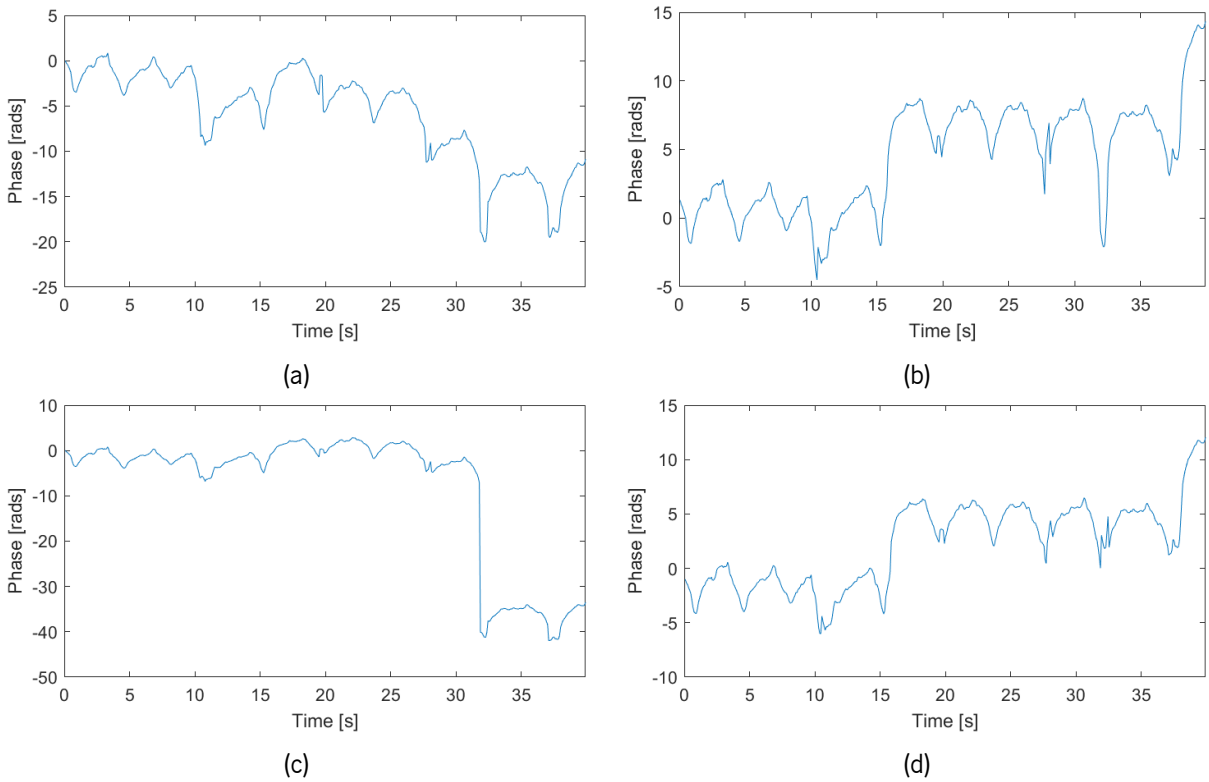

Figure 29: Example of a chest movement signal obtained from the same data using different combinations of techniques: a) Single chirp and DACM; b) Single chirp and phase correction; c) Differential and DACM; d) Differential and phase correction.

In Figure 30, the FFTs of the signals in Figure 29 can be seen. Within this figure, Figure 30a corresponds to the FFT of the signal in Figure 29a, Figure 30b corresponds to the FFT of the signal in Figure 29c, Figure 30c corresponds to the FFT of the signal in Figure 29c and Figure 30d corresponds to the FFT of the signal in Figure 29d. In each of these subfigures, the green dashed lines represent the limits of the RR peak detection interval, the red dashed lines represent the limits of the HR peak detection interval, the green circle represents the RR peak and the red circle represents the HR peak.

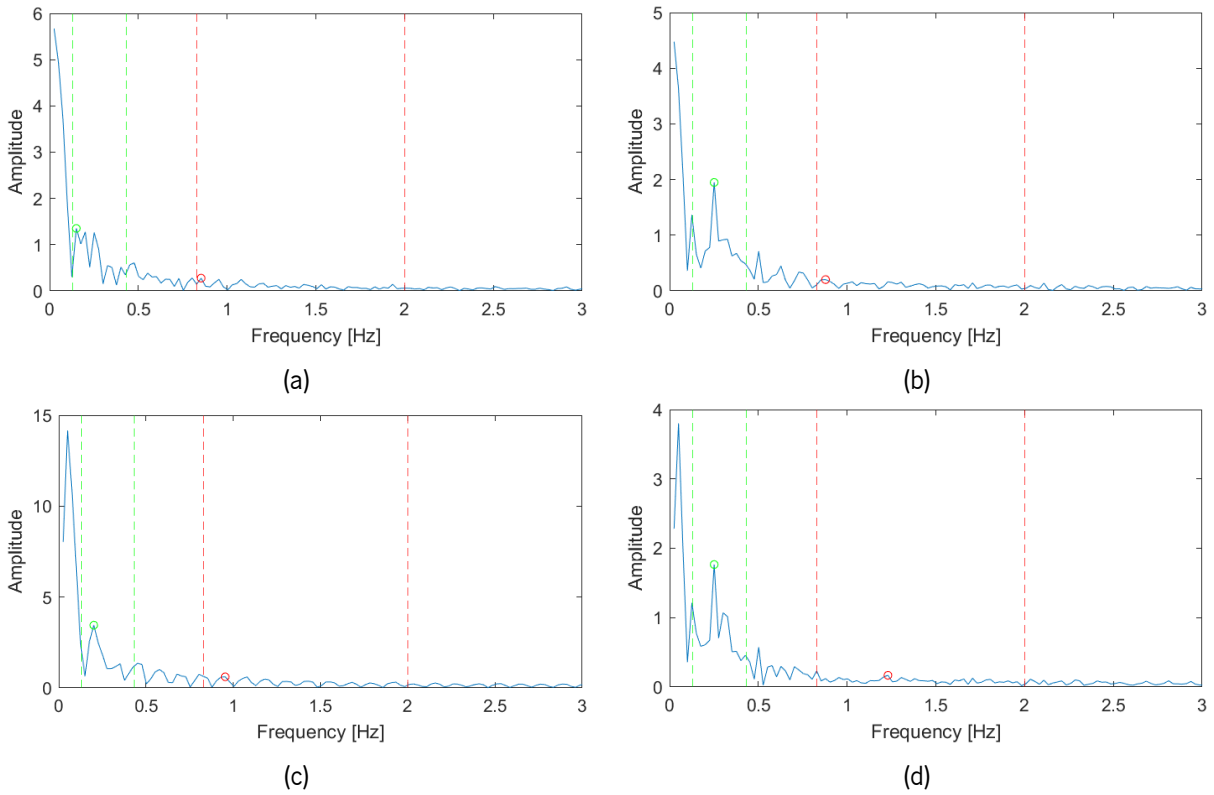

Figure 30: Example of the FFT of a chest movement signal obtained from the same data using different combinations of techniques: a) Single chirp and DACM; b) Single chirp and phase correction; c) Differential and DACM; d) Differential and phase correction.

On Table 8 the results for set 1 of raw data recordings can be seen, with separate MRE for each recording, vital sign, and combination of algorithms: single chirp data with phase correction, single chirp data with DACM algorithm, differential data with phase correction and differential data with DACM algorithm. On Table 9, the results for set 2 of raw data recordings can be seen, with the same structure as Table 8. In both of these tables, the lowest MRE for each vital sign in each recording is highlighted in bold. For these results, average MRE scores were not calculated due to there only being two raw data recordings for each situation in each set.

Table 8: Performance of the different variations of the algorithm in measuring vital signs based on set 1 of raw data.

			DACM		Phase correction	
			RR MRE (%)	HR MRE (%)	RR MRE (%)	HR MRE (%)
Stationary vehicle recordings	Rec.1	Single Chirp	13.62	6.07	13.49	5.69
		Differential	**10.38**	**5.37**	11.07	7.87
	Rec. 2	Single Chirp	20.36	7.18	19.22	10.69
		Differential	**9.78**	**3.51**	14.38	6.39
Moving vehicle recordings	Rec.1	Single Chirp	12.75	6.49	11.91	22.92
		Differential	**3.75**	**5.42**	13.67	7.53
	Rec. 2	Single Chirp	**12.67**	7.66	15.02	14.19
		Differential	16.88	9.11	14.35	**4.11**

Table 9: Performance of the different variatons of the algorithm in measuring vital signs based on set 2 of raw data.

			DACM		Phase correction	
			RR MRE (%)	HR MR (%)	RR MRE (%)	HR MRE (%)
Stationary vehicle recordings	Rec.1	Single Chirp	17.52	**3.68**	**17.35**	4.21
		Differential	17.73	4.69	17.95	3.84
	Rec. 2	Single Chirp	10.52	3.73	**9.38**	2.66
		Differential	9.89	3.27	10.03	**2.54**
Moving vehicle recordings	Rec.1	Single Chirp	**9.95**	9.43	16.92	5.37
		Differential	16.84	**4.13**	16.17	6.83
	Rec. 2	Single Chirp	33.76	10.55	35.53	**8.03**
		Differential	30.28	10.96	**24.03**	10.70

5.3.2 Discussion

In this bioradar, there are multiple combinations of radar settings and algorithm variants that are being tested, as there are three parts of the process which have two different techniques. These parts are the raw data acquisition, for which there are two different settings as can be seen in Table 4, the used chirp

data, that can be single chirp or differential between two chirps, and phase unwrapping, which can be made through the DACM algorithm or phase correction.

In Figure 29, a chest movement signal obtained using different combinations of used chirp data and phase unwrapping algorithm, but based on the same raw radar data from one of the stationary vehicle recordings, is displayed. In all of the signals, the respiratory component is apparent in the larger oscillations, and, within each respiratory cycle, smaller oscillations can also be observed, that seem consistent between signals, which correspond to the heartbeat component of the signal. However, in the sections between each respiratory cycle, there are differences between signals. In Figure 29c, there is a very large discontinuity at around 32 seconds in which the phase drops significantly, seemingly between two consecutive frames. This cannot correspond to the subject's chest movement, as it is too fast and sudden, and therefore must be related to an error in phase unwrapping that is not present in any of the other signals. In Figures 29a and 29b there are also sudden decreases in detected phase at around the same time, however, they are not as steep as the the one in Figure 29c and the signal recovers slightly (Figure 29a) or fully (Figure 29b) after the drop so this could therefore reasonably correspond to the subject's chest movement. There are other situations in which the signals differ from each other, such as changes in the subject's base range between respiratory cycles, such as the ones at around 15 seconds in Figures 29d and 29d, or smaller inconsistencies between signals. Overall it appears that phase correction offers a stabler signal, and that the DACM algorithm is more prone to unwrapping errors that affect the subject's base range, as can be seen in Figures 29a and 29b. As for the used chirp data, comparing the signals obtained using phase correction, the signal that uses single chirp data (Figure 29b) has a large dip at around 32 seconds, that is not present in the signal that uses the differential data technique (Figure 29d), and instead is replaced with oscillations that could be related to heartbeat, but could also be noise. Overall, all the combinations appear to contain clear respiratory and heartbeat components, despite some inconsistencies and irregularities, with differential data and phase correction appearing to provide the most stable signal.

The effects of each combination of techniques when performing the FFT of the chest movement signal can be seen in Figure 30. Here it clear that the used techniques have an impact in vital sign measurement. First of all, it is clear that the discontinuities exhibited by the signals obtained using DACM (Figures 29a and 29c) have a negative effect in measuring both vital signs, as can be seen in Figures 30a and 30c, where harmonics caused by the discontinuities end up dominating the spectrum, especially in Figure 30a, which corresponds to the signal with largest discontinuity, obtained using differential data and the DACM algorithm. The FFTs of the signals obtained using the phase correction technique (Figures 29b and 29d),

which do not have discontinuities like the previously discussed signals, are in Figures 30b and 30d. The detected RR peak is the same for both cases, however, there is no clear HR peak in either FFT, and the detected HR peak is very different between the two. Based on these observations, it can be said that the phase correction algorithm should have better results, due to being less prone to inserting discontinuities in the chest movement signal, however, it seems that HR measurement is an issue. Nevertheless, these observations are based on a single segment of chest movement signal, and might not be representative of the performance of these algorithms.

The results for this bioradar are displayed in Table 8, for set 1 of raw data recordings and in Table 9 for set 2 of raw recordings. Besides the two different sets that were obtained with different recording characteristics, the results are further split by the used chirp data and phase unwrapping method. Firstly, the results of each set of data will be analyzed separately, and then the two sets will be compared.

For set 1 of raw data, whose results are displayed in Table 8, when looking at the results from the stationary vehicle recordings, the RR and HR measurements with the least MRE, for both recordings, were the ones performed using the differential between chirps and the DACM algorithm. This is also true for the first moving vehicle recording, however, for the second moving vehicle recording, the best results for RR and HR are not using the same combination of techniques, as the best RR measurement performance is obtained using single chirp data and the DACM algorithm and the best HR measurement performance is obtained using differential chirp data and phase correction. However, in general, it can be said that the best performance for this set of data, for both vital signs, is obtained using differential chirp data and the DACM algorithm. This goes against what was expected after analyzing the chest movement signals from Figure 29, and might be due to the FFT method being robust against discontinuities and shifts in the baseline of the signal.

For set 2 of raw data, whose results are displayed in Table 9, the results are much more varied between data recordings, with seemingly no clear pattern to determine what is the best variation of the algorithm. For the stationary vehicle recordings, the average MRE for each vital sign and algorithm combination can be calculated. Taking this into account, the best RR measurements performance when the vehicle is stationary is achieved using single chirp data with phase correction, as that combination has the best RR measurement performance in both stationary vehicle recordings. The best HR measurement performance when the vehicle is stationary is achieved using differential chirp data and phase correction, with an average MRE of 3.19 %. As for the moving vehicle recordings, when comparing the results in general, it can be concluded that the second recording must have had exceptionally bad conditions for RR measurement, since the MRE values for the measurements of this vital sign in that data recording are much higher than

for any data recording made using this bioradar. Because of this, the results from this recording should be discarded when analyzing RR measurement performance, leaving only the results from the first moving vehicle data recording. Analyzing the remaining data recording, the best RR measurement performance comes from using single chirp data and the DACM algorithm, and, analyzing both recordings, the best HR measurement performance comes from using single chirp data and the phase correction algorithm, with an average MRE of 6.70 %. In general, for this set of data, it can be said that phase correction appears to be the best phase unwrapping method, as it has better performance in all situations except when measuring RR when the vehicle is in motion. As for the used chirp data, single chirp is better when evaluating RR, as for both vehicle situations it yields better results. On the other hand, when evaluating HR, differential data has better performance when the vehicle is stationary but single chirp data has better performance when the vehicle is in motion. However, as the data from the second moving vehicle recording had bad conditions for RR, the HR measurements could also have been affected. Therefore, the stationary vehicle results should be taken more into account. Due to this, it will be considered that the best algorithm variations for this set of data are single chirp with phase correction for RR measurements and differential data with phase correction for HR measurements, which is more in line with the analysis made to the chest movement signals in Figure 29 and the FFTs in Figure 30.

Comparing the performance of measurements between the two sets of data, it appears that the data from set 1 was better for RR measurements when the vehicle is stationary, with an average of 10.08 % MRE, obtained using differential data and the DACM algorithm, in comparison to 13.37 % average MRE obtained from the stationary vehicle recordings of set 2 using single chirp data with phase correction. When the vehicle is in motion, set 2 has better performance when measuring RR using single chirp data and the DACM algorithm if the second recording is ignored, since the first recording, using these techniques, has an MRE of 9.95 % while in set 1 the average MRE for this situation is 10.32 %, using differential data and the DACM algorithm. As for the other vital sign, set 2 results in better performance in measuring HR when the vehicle is stationary with an average of 3.19 % MRE using differential data with phase correction in comparison to 4.44 % average MRE from set 1 using differential data and the DACM algorithm. When the vehicle is in motion, set 1 has better performance than set 2, with an average of 5.82 % MRE when using differential data with phase correction. Because, as previously established, stationary vehicle results should be taken into account more than moving vehicle results, it is concluded that set 1 has better RR measurement performance by using differential data and the DACM algorithm, and set 2 has better HR measurement performance by using differential data and phase correction. The main difference between these sets was the framerate of the recordings, with set 2 having 12 frames per second and set 1 only

8. The higher framerate might have a great impact on the HR measurement performance, as a lower framerate complicates detection of the quick pulses associated with heartbeat.

This bioradar's results are, in general, better for HR measurements than RR measurements, suggesting that it is better at measuring HR than RR. This could be because the RR of a person is more variable than HR, and there are also less respiratory cycles than cardiac cycles in the time window that is used for a single measurement, since a respiratory cycle takes longer than a cardiac cycle, and both of these factors affect RR measurements. The use of differential data also provides better HR measurements than single chirp data, this could be because the differential technique eliminates clutter, which is a big problem when measuring HR. Furthermore, for set 1 of radar data, differential data consistently provides better results than single chirp data on both moving vehicle recordings, indicating that it might be effective at reducing the noise caused by the vehicle's movement. Lastly, it should be taken into account that these results are based on a very small sample size of only two data recording for each vehicle status in each recording set, and could be misleading because of this.

5.4 Bioradar Comparison

After analyzing the performance of each bioradar separately, they can now be compared to each other to determine which is the best option for vital sign measurement.

When the vehicle is stationary, the best RR measurement results come from the Ancho bioradar when using a loopback filter as the static background clutter removal method (6.28 % average MRE) and the best HR measurement results come from set 2 of the RIC60A bioradar when using differential data and phase correction as the unwrapping method (3.19 % average MRE). When the vehicle is in motion, the best RR measurement results come once again from the Ancho bioradar when using a loopback filter as the static background clutter removal method (8.83 % average MRE) and the best HR measurement results come from set 1 of the RIC60A bioradar when using differential data and phase correction as the phase unwrapping method (5.82 % average MRE). Overall, this indicates that the Ancho bioradar is better at measuring RR, while the RIC60A bioradar is better at measuring HR. This could indicate that the IR-UWB radar technology is better at capturing the larger chest movements associated with respiration while FMCW radar technology is better at capturing the smaller chest movements associated with HR, because of the precise range resolution that this technology enables through phase analysis. On the other hand, the Ancho bioradar having better performance than the RIC60A bioradar when measuring RR could be due

to the former having a higher framerate, or simply due to the latter being prone to having discontinuities between respiratory cycles even after phase unwrapping that could be interfering with RR measurements more than HR measurements. The best methods and their respective results for each bioradar are in table 10. In this table, the best method row for the Xandar Kardian bioradar is left blank because no alternative methods were tested for that bioradar.

Table 10: Best methods and their respective results for each radar and each vital sign.

			Ancho bioradar	Xandar Kardian bioradar	RIC60A bioradar
Stationary vehicle	RR	Best method	Loopback filter	-	Set 1 Differential data DACM algorithm
		Avg. MRE (%)	6.28	14.38	10.08
	HR	Best method	Loopback filter	-	Set 2 Differential data Phase correction
		Avg. MRE (%)	3.96	16.83	3.19
Moving vehicle	RR	Best method	Loopback filter	-	Set 2 Single chirp data DACM algorithm
		Avg MRE (%)	8.83	12.00	9.95
	HR	Best method	Loopback filter	-	Set 1 Differential data Phase correction
		Avg MRE (%)	9.98	44.73	5.82

The Xandar Kardian bioradar had worse results than the other bioradars in every situation, even though it is also based on IR-UWB technology like the Ancho bioradar. Because the Ancho bioradar that uses similar radar technology has better results, it appears that the employed algorithm is what makes the difference between these two bioradars. Thus, a method of measuring the vital signs over a larger window of time, like what is done using the Ancho bioradar, is better in an automotive environment than attempting to make instantaneous measurements, like the Xandar Kardian bioradar appears to do. Due to the fact that the RR and HR measurements are instantaneous, it can be speculated that this bioradar's algorithm is

based on peak detection. If that is the case, it is very prone to being affected by noise, especially when trying to measure HR, and therefore does not function well at all in an automotive environment, much less when the vehicle is in motion.

Chapter 6

Conclusions and Future Work

In this, chapter, the conclusions and future work of this study are presented. It is divided into two sections, one for the conclusions and another for future work.

6.1 Conclusions

The goal of this study was the development of a bioradar capable of measuring RR and HR in an automotive environment. To reach this goal, algorithms for two different bioradars, one that is based on IR-UWB radar technology and another that is based on FMCW radar technology, were developed, and tested in an automotive environment, together with a commercially available bioradar that also has RR and HR measurement capabilities, adapted by the manufacturer to work better in an automotive environment. The obtained results are promising, but they are still not good or consistent enough, and there are problems that need to be addressed, such as the sensibility of the bioradars to body movement and respiration harmonics, before any of the developed bioradars can be considered reliable for vital sign measurements in an automotive environment. The best results for each vital sign are also not from the same bioradar, which means that, from the explored bioradars and techniques, there is no single bioradar that would provide the best RR and HR measurements at the same time. Nevertheless, the results obtained from the developed bioradars are better than the results obtained from the commercially available bioradar. The results are not very comparable to existing literature, as an automotive environment is very different from the usual environment where such bioradars are tested, and even among the studies made in automotive environments, the setup is very different to what was used.

Two different algorithm variations were tested for the Ancho bioradar. Of these two, the variation that

uses a loopback filter for static background clutter removal had a better performance in measuring both RR and HR in both vehicle situations, stationary and in motion. The performance when the vehicle is moving in worse than when the vehicle is stationary, especially when measuring HR, as the average MRE increases from less than 5 % to almost 10 %. This bioradar, using the loopback filter, had the best RR measuring performance of all the bioradars.

The Xandar Kardian presence detection with vital sign monitoring had very underwhelming results, having an MRE above 10 % for both vital signs when the vehicle is stationary, even after adjusting the results to take into account the reliability metric provided by the bioradar. When the vehicle is in motion, the MRE of RR measurements actually decreased, which is the opposite of what happened in all the other bioradars, even though the average reliability decreased dramatically. The MRE of HR measurements increased to above 40 % when the vehicle is in motion, indicating that this bioradar is incapable of measuring HR at all when the vehicle is in motion. This suggests that instantaneous measurements of RR and HR are not viable in an automotive environment, at least in their current state.

For the RIC60A bioradar, multiple variations of the algorithm were tested, as well as two separate sets of data recordings obtained using different recording settings. The results of this bioradar were that set 1, which has less framerate but better signal quality, provided better RR measurement results when using differential data and the DACM algorithm, and that set 2, which has a higher framerate at the expense of signal quality, provided better HR measurement results when using differential data and phase correction. The HR measurement performance of this bioradar was the best of the tested bioradars.

Measurement performance, in general, is worse when the vehicle is in motion than when it is stationary, which is due to there being more interference when the vehicle is moving and was expected. This increase in interference is mainly due to the body movement of the subject, that increases when the vehicle is in motion as there is involuntary body motion when the vehicle curves, accelerates and brakes. Besides this, the movement of the vehicle and the vibrations caused by the motor can also shake the radar, which will affect the quality of the received data more or less depending on how the radar is fixed to the inside of the vehicle.

In the end, the results are based on a very small amount of data, from a single subject and always in the same environment, so the sample size is not only small, but also not varied at all. This is even more apparent for the RIC60A bioradar, which only has two data recordings for each vehicle status in each recording set, and one of the recordings for set 2 had a particularly bad performance in RR measurement probably due to especially bad conditions, resulting in this set effectively only having one data recording to evaluate moving vehicle RR measurement performance. Because of this, the results could be misleading,

as a larger amount of data with more variation of vehicles and subjects would provide more concrete results.

6.2 Future Work

Future work would be focused on trying to overcome the challenge of moving vehicle vital sign measurements by implementing techniques to detect body movement and reduce its impact on the vital sign measurement, as that is the main cause of interference. However, the used techniques should not be too resource intensive, as the bioradar should be able to consistently output RR and HR measurements. Furthermore, more data could be acquired from different subjects and in different vehicles, in order to build a larger and more diverse dataset, that would be more useful to evaluate which techniques are more effective.

Particularly for the RIC60A bioradar, more data collection settings could be explored, specifically further increasing framerate, to try and achieve even better results. Other noise canceling techniques could also be experimented with, to try to improve the quality of the detected chest movement signal, and try to remove discontinuities such as the ones that were observed in the results of this study.

Another aspect that could be explored is HRV measurement. For this, the HR measuring technique would have to be changed or adapted to instead measure how much time passes between individual heartbeats, so that an HRV metric could be calculated. This was not tried because there needs to be a clear heartbeat signal in order to achieve this, which would require more filtering of the chest movement signal that is currently too noisy to reliably make this sort of measurement, and, for this type of metric, the compounding of small measurement errors results in major discrepancies from reality. In order to do this, the framerate of the used bioradar would also need to be improved, so that the measurement of time between heartbeats is more precise.

Bibliography

[1] S. Narayanan, E. Chaniotakis, and C. Antoniou, "Shared autonomous vehicle services: A comprehensive review," *Transportation Research Part C: Emerging Technologies*, vol. 111, pp. 255–293, 2020.

[2] M. A. Cretikos, R. Bellomo, K. Hillman, J. Chen, S. Finfer, and A. Flabouris, "Respiratory rate: The neglected vital sign," *Medical Journal of Australia*, vol. 188, no. 11, pp. 657–659, 2008.

[3] P. Palatini and S. Julius, "Elevated heart rate: A major risk factor for cardiovascular disease," *Clinical and experimental hypertension*, vol. 26, no. 7-8, pp. 637–644, 2004.

[4] Y. Zhang, F. Qi, H. Lv, F. Liang, and J. Wang, "Bioradar technology: Recent research and advancements," *IEEE Microwave Magazine*, vol. 20, no. 8, pp. 58–73, 2019.

[5] J. G. Betts, K. A. Young, J. A. Wise, *et al.*, *Anatomy and Physiology*. OpenStax, 2013.

[6] A. Ratnovsky, D. Elad, and P. Halpern, "Mechanics of respiratory muscles," *Respiratory physiology & neurobiology*, vol. 163, no. 1-3, pp. 82–89, 2008.

[7] G. J. Tortora and B. H. Derrickson, *Principles of anatomy and physiology*. John Wiley & Sons, 2018.

[8] F. Shaffer and J. P. Ginsberg, "An overview of heart rate variability metrics and norms," *Frontiers in public health*, p. 258, 2017.

[9] G. Nazari, J. C. MacDermid, K. E. Sinden, J. Richardson, and A. Tang, "Reliability of zephyr bioharness and fitbit charge measures of heart rate and activity at rest, during the modified canadian aerobic fitness test, and recovery," *The Journal of Strength & Conditioning Research*, vol. 33, no. 2, pp. 559–571, 2019.

[10] G. Nazari and J. C. MacDermid, "Reliability of zephyr bioharness respiratory rate at rest, during the modified canadian aerobic fitness test and recovery," *The Journal of Strength & Conditioning Research*, vol. 34, no. 1, pp. 264–269, 2020.

[11] M. A. Richards, J. A. Scheer, and W. A. Holm, *Principles of Modern Radar*. SciTech Publishing, 2010, ISBN: 978-1-891121-52-4.

[12] M. I. Skolnik, *Introduction to Radar Systems*, Second. McGraw-Hill, 1981, ISBN: 0-07-057909-1.

[13] E. Antolinos, F. García-Rial, C. Hernández, D. Montesano, J. I. Godino-Llorente, and J. Grajal, "Cardiopulmonary activity monitoring using millimeter wave radars," *Remote Sensing*, vol. 12, no. 14, p. 2265, 2020.

[14] Y. Rong and D. W. Bliss, "Direct rf signal processing for heart-rate monitoring using uwb impulse radar," in *2018 52nd Asilomar Conference on Signals, Systems, and Computers*, IEEE, 2018, pp. 1215–1219.

[15] W. H. Lee, J. Y. Na, H. J. Lee, *et al.*, "Analysis of heart rate variability using impulse radio ultra-wideband radar in neonatal intensive care unit," in *2019 IEEE SENSORS*, IEEE, 2019, pp. 1–4.

[16] W. Yin, X. Yang, L. Li, L. Zhang, N. Kitsuwan, and E. Oki, "Hear: Approach for heartbeat monitoring with body movement compensation by ir-uwb radar," *Sensors*, vol. 18, no. 9, p. 3077, 2018.

[17] Y. Lee, J.-Y. Park, Y.-W. Choi, *et al.*, "A novel non-contact heart rate monitor using impulse-radio ultra-wideband (ir-uwb) radar technology," *Scientific reports*, vol. 8, no. 1, pp. 1–10, 2018.

[18] E. Pittella, A. Bottiglieri, S. Pisa, and M. Cavagnaro, "Cardiorespiratory frequency monitoring using the principal component analysis technique on uwb radar signal," *International Journal of Antennas and Propagation*, vol. 2017, 2017.

[19] C. Ding, J. Yan, L. Zhang, H. Zhao, H. Hong, and X. Zhu, "Noncontact multiple targets vital sign detection based on vmd algorithm," in *2017 IEEE Radar Conference (RadarConf)*, IEEE, 2017, pp. 0727–0730.

[20] F. Khan and S. H. Cho, "A detailed algorithm for vital sign monitoring of a stationary/non-stationary human through ir-uwb radar," *Sensors*, vol. 17, no. 2, p. 290, 2017.

[21] Z. Yang, M. Bocca, V. Jain, and P. Mohapatra, "Contactless breathing rate monitoring in vehicle using uwb radar," in *Proceedings of the 7th International Workshop on Real-World Embedded Wireless Systems and Networks*, 2018, pp. 13–18.

[22] S. K. Leem, F. Khan, and S. H. Cho, "Vital sign monitoring and mobile phone usage detection using ir-uwb radar for intended use in car crash prevention," *Sensors*, vol. 17, no. 6, p. 1240, 2017.

[23] M. Arsalan, A. Santra, and C. Will, "Improved contactless heartbeat estimation in fmcw radar via kalman filter tracking," *IEEE Sensors Letters*, vol. 4, no. 5, pp. 1–4, 2020.

[24] L. Sun, S. Huang, Y. Li, *et al.*, "Remote measurement of human vital signs based on joint-range adaptive eemd," *IEEE Access*, vol. 8, pp. 68 514–68 524, 2020.

[25] Y. Wang, W. Wang, M. Zhou, A. Ren, and Z. Tian, "Remote monitoring of human vital signs based on 77-ghz mm-wave fmcw radar," *Sensors*, vol. 20, no. 10, p. 2999, 2020.

[26] M. Alizadeh, G. Shaker, and S. Safavi-Naeini, "Experimental study on the phase analysis of fmcw radar for vital signs detection," in *2019 13th European Conference on Antennas and Propagation (EuCAP)*, IEEE, 2019, pp. 1–4.

[27] G.-W. Fang, C.-Y. Huang, and C.-L. Yang, "Simultaneous detection of multi-target vital signs using eemd algorithm based on fmcw radar," in *2019 IEEE MTT-S International Microwave Biomedical Conference (IMBioC)*, IEEE, vol. 1, 2019, pp. 1–4.

[28] A. Ahmad, J. C. Roh, D. Wang, and A. Dubey, "Vital signs monitoring of multiple people using a fmcw millimeter-wave sensor," in *2018 IEEE Radar Conference (RadarConf18)*, IEEE, 2018, pp. 1450–1455.

[29] D. Zhang, M. Kurata, and T. Inaba, "Fmcw radar for small displacement detection of vital signal using projection matrix method," *International Journal of Antennas and Propagation*, vol. 2013, 2013.

[30] M. E. Torres, M. A. Colominas, G. Schlotthauer, and P. Flandrin, "A complete ensemble empirical mode decomposition with adaptive noise," in *2011 IEEE international conference on acoustics, speech and signal processing (ICASSP)*, IEEE, 2011, pp. 4144–4147.

[31] Q. T. Tran, T. L. Ton, N. T. M. Nguyen, and B. D. Nguyen, "A k-band noninvasive vital signs monitoring system in automotive applications," in *2019 International Symposium on Electrical and Electronics Engineering (ISEE)*, IEEE, 2019, pp. 85–88.

[32] F. J. Harris, "On the use of windows for harmonic analysis with the discrete fourier transform," *Proceedings of the IEEE*, vol. 66, no. 1, pp. 51–83, 1978.